DOKUZ EYLÜL UNIVERSITY

GRADUATE SCHOOL OF NATURAL AND APPLIED SCIENCES

FALL DETECTION AND ACTIVITY RECOGNITION

by

Alican ESLEK

September, 2014

İZMİR

FALL DETECTION AND ACTIVITY RECOGNITION

A Thesis Submitted to the
Graduate School of Natural and Applied Sciences of Dokuz Eylül University
In Partial Fulfillment of the Requirements for Master of
Science in Electrical and Electronics Engineering

by
Alican ESLEK

September, 2014

İZMİR

THESIS EXAMINATION RESULT FORM

We have read the thesis entitled **"FALL DETECTION AND ACTIVITY RECOGNITION"** completed by **ALİCAN ESLEK** under supervision of **ASST. PROF. DR. YAVUZ ŞENOL** and we certify that in our opinion it is fully adequate, in scope and in quality, as a thesis for the degree of Master of Science.

Asst. Prof. Dr. Yavuz ŞENOL

Supervisor

Prof.Dr. Uğur ÇAM

(Jury Member)

Assoc.Prof.Dr. Zeki KIRAL

(Jury Member)

Prof.Dr. Ayşe OKUR
Director
Graduate School of Natural and Applied Sciences

ACKNOWLEDGEMENTS

I would like to thank my advisor, Asst. Prof. Dr. Yavuz ŞENOL, whose knowledge and guidance have helped me get through the hard process while preparing this project.

I would also express my gratitude towards my parents whose love and support have been the greatest asset in my life as well in this thesis.

I have to specially thank Gökmen AŞCIOĞLU, who has worked with me a lot about data collection and software development on mbed NXP LPC1768 microcontroller. Also, I am grateful to all volunteers who gave their time to this project.

Alican ESLEK

FALL DETECTION AND ACTIVITY RECOGNITION

ABSTRACT

Recently the problems connected with the ageing population all over the world have become more and more severe. Many projects have been developed to enable people to live longer in home environment, thus keeping their independence together with reducing the expenses of the public health care. Falls are dangerous for the aged population as they can adversely affect health; it can result in critical injuries like hip fractures. Immobilization caused by injury or unconsciousness means that the victim cannot summon help themselves. The most common falls occur when the person is alone and unable to get up, resulting in long lies which are associated with institutionalisation and high morbidity-mortality rate. The feeling of fall increases the anxiety and the depression in the elderly. Hence, an automatic fall detection system is an important setting. Though various pilot applications and commercial fall detection systems exist, the real-life validation of these systems is scant.

Our study has focused on developing new method for detection of fall to be adapted for real-life applications among older people. Fall detection system has the capability of automatically discriminating between a fall-event and an activities daily living (ADL). In this study, a wearable monitoring device, based on tri-axial accelerometer and gyroscope, is placed at the centre of the chest to collect real-time fall data. Also, it consists of Bluetooth module that links wirelessly with a laptop and GPS (Global Positioning System) module to inform medical attention using location information of the victim. The proposed algorithm, coupled with accelerometers and gyroscopes, reduces both false positives and false negatives, while improving fall detection accuracy. The proposed solution features low computational cost and real-time response.

Keywords: Acceleration, gyroscope, fall detection, angular velocity

DÜŞME TESPİTİ VE AKTİVİTELERİN BELİRLENMESİ

ÖZ

Son yıllarda yaşlı insanlarla ilgili problemler giderek daha da önem kazanmaktadır. Bu insanların ev ortamında yalnız rahatça yaşayabilmeleri, bağımsız hareket edebilmeleri ve sağlık masraflarını düşürmeleri amacıyla birçok proje geliştirilmiştir. Bu problemlerin başında düşme olayları gelmektedir ve bu düşme durumu kalça kemiği kırılması gibi insan sağlığını ölümcül derecede etkileyecek sonuçlar doğurmaktadır. Düşme sonucu meydana gelen sakatlanma veya bilinç kaybından dolayı insan hareket edebilme kabiliyetini kaybeder ve yardım çağıramayacak duruma gelebilir. Bu insanların düşmeye bağlı olarak uzun süre yerde hareketsiz kalması sakatlanma ve ölüm oranlarını ciddi şekilde artırmaktadır. Bu düşme olayları ayrıca yaşlı insanlarda korku, endişe ve depresyon gibi psikolojik etkiler yaratmaktadır. Bu düşüncelerden yola çıkarak gerçek zamanlı otomatik düşme tespiti yapan cihazlar çok önemli hale gelmektedir. Bu cihazlarla ilgili ticari hale gelmiş veya deneme aşamasında olan çalışmalar olmasına rağmen halen daha günümüzde yaygın olarak kullanılmamaktadır.

Bizim çalışmamız düşme tespiti konusunda yeni bir metot ve güçlü bir düşme algoritmasına sahip düşme tespiti cihazı geliştirmeye odaklanmıştır. Düşme tespiti cihazımız günlük aktivitelerimizle (yürüme, koşma, oturma vb) düşme olayını ayırt edebilme kabiliyetine sahiptir. Bu cihaz insan vücudunda göğüs boşluğuna yerleştirilebilir şekilde tasarlanmış olup, gerçek zamanlı düşme verilerini almak için ivme ve jiroskop algılayıcıları kullanmaktadır. Ayrıca bu verileri bilgisayar ortamına aktarmak için Bluetooth cihazı kullanılmıştır. Buna ek olarak düşen kişiye tıbbi yardım götürebilmek için konum bilgileri GPS cihazı kullanılarak alınmaktadır. Bizim algoritmamız ivme ve jiroskop verilerini birlikte kullanarak düşme tespitini daha doğru ve kesin bir şekilde gerçekleştirmeyi amaçlamaktadır. Ayrıca bu sistem gerçek zamanlı olup, düşük hesaplama yüküne sahiptir.

Anahtar kelimeler: İvme, jiroskop, düşme tespiti, açısal hız

CONTENTS

Page

THESIS EXAMINATION RESULT FORM ii
ACKNOWLEDGEMENTS iii
ABSTRACT iv
ÖZ v
LIST OF FIGURES ix
LIST OF TABLES xi

CHAPTER ONE - INTRODUCTION 1

1.1 Introduction 1
1.2 Outline of Thesis 3

CHAPTER TWO – MATERIALS AND ITS FEATURES 4

2.1 Accelerometer 4
2.1.1 General Description 4
2.1.2 Communication Interface 5
2.1.3 Reading Output Data 6
2.1.4 Initalization 6
2.2 Gyroscope 8
2.2.1 General Description 8
2.2.2 Communication Interface 9
2.2.3 Reading Output Data 9
2.2.4 Initalization 9
2.3 Bluetooth 11
2.3.1 General Description 11
2.3.2 Configuration 11
2.4 Global Positioning System (GPS) 13
2.4.1 General Description 13
2.4.2 Features 13

2.5 Vodafone Vodem K3770 14
2.5.1 General Description 14
2.6 Microcontroller Unit 15
2.6.1 General Description 15
2.6.2 Features & Benefits 15
2.6.2.1 Features 15
2.6.2.2 Benefits 16
2.6.3 LPC1768 Microcontrollers 16
2.7 Peripherals 18
2.7.1 Buzzer 18
2.7.2 Button 19
2.7.3 Led 19
2.7.4 Battery 20
2.7.5 Housing 20

CHAPTER THREE – SYSTEM DESIGN 21

3.1 Hardware Implementation 21
3.1.1 OrCAD 21
3.1.1.1 Schematic 21
3.1.1.2 Steps to Export Design to Layout 22
3.1.1.3 Layout 22
3.2 Software Implementation 26
3.2.1 I^2C Interface 27
3.2.1.1 Start (S) and Stop (P) Conditions 28
3.2.1.2 Data Format / Acknowledge 28
3.2.1.3 Communications 29
3.2.2 Asynchronous Serial Communication Interface 31

CHAPTER FOUR – FALL DETECTION ALGORITHM 34

4.1 Fall Detection Algorithm Parameters 34
4.1.1 Threshold-Based Analysis for Acceleration Magnitude 35

4.1.2 Vertical Velocity Estimate Analysis 38
4.1.2.1 Numerical Integration 40
4.1.2.2 Integration Drift 42
4.1.3 Body Posture Analysis 43
4.1.4 Threshold-Based Analysis for Angular Velocity 45
4.2 Fall Detection Algorithm 46
4.2.1 The Proposed Fall Detection Algorithm 47

CHAPTER FIVE - SIMULATION RESULTS 50

5.1 Recording and Experimental Set-up 50
5.2 Intentional Falls and Sequential ADL in Laboratory Environment 51
5.3 Test Results 53

CHAPTER SIX – CONCLUSIONS AND FUTURE WORK 62

REFERENCES 64

LIST OF FIGURES

Page

Figure 2.1 ADXL345 system block diagram and pin designations 4
Figure 2.2 Recommended connections for I^2C mode 5
Figure 2.3 Data construction 6
Figure 2.4 Initialization sequence 7
Figure 2.5 ITG-3200 system block diagram and pin designations 8
Figure 2.6 Initialization sequence 10
Figure 2.7 JY-MCU Bluetooth module 11
Figure 2.8 Module configuration connections 12
Figure 2.9 EM-406A GPS receiver engine board 13
Figure 2.10 Vodafone vodem K3770 14
Figure 2.11 mbed NXP LPC1768 prototyping board 15
Figure 2.12 CEM-1203(42) magnetic buzzer 18
Figure 2.13 Pulse width modulation (PWM) technique 18
Figure 2.14 Push Button 19
Figure 2.15 Li-Po Battery 20
Figure 2.16 Housing 20
Figure 3.1 Block diagram of the system 21
Figure 3.2 Library manager for example footprint 23
Figure 3.3 Top layer routing of the PCB 25
Figure 3.4 Bottom layer routing of the PCB 25
Figure 3.5 Placement of parts of the PCB 26
Figure 3.6 mbed compiler 27
Figure 3.7 START and STOP conditions 28
Figure 3.8 Acknowledge on the I^2C bus 29
Figure 3.9 Complete I^2C data transfer 30
Figure 3.10 Single-byte and multiple-byte write sequence 30
Figure 3.11 Single-byte and multiple-byte read sequence 31
Figure 3.12 Serial frame, some symbols in the frame have configurable bit sizes 32
Figure 4.1 The four phases of a fall event 35
Figure 4.2 Anatomy of a fall 37

Figure 4.3 Integration areas to calculate vertical velocity 39
Figure 4.4 Integration using rectangular and trapezoidal methods 41
Figure 4.5 Discrete acceleration values 41
Figure 4.6 Method for determining the body posture of the faller 43
Figure 4.7 Graphical operation of the method for determining chest posture angle.. 45
Figure 4.8 The proposed fall detection algorithm 49
Figure 5.1 Recording and experimental set-up 50
Figure 5.2 Sample signals of walking, sit-stand, lie-stand and backward fall for young volunteer-1 (Alican). The signals displayed are (a) the Root-Sum-of-Squares (RSS) of acceleration magnitude, (b) vertical velocity estimate, (c) dot-product angle and (d) angular velocity 58

LIST OF TABLES

Page

Table 2.1 AT commands 12
Table 2.2 Features of NXP LPC1768 microcontroller... 17
Table 5.1 Threshold values and units of the different parameters for the proposed fall detection algorithm 59
Table 5.2 Sensitivity (%) and specificity (%) values of the proposed fall detection algorithm... 61
Table 5.3 False positive (FP) quantities and false positive rate (FP/hour) and false positives per day (FP/day) for the proposed fall detection algorithm tested against the recorded continuous unscripted ADL..................................... 61

CHAPTER ONE
INTRODUCTION

1.1 Introduction

The proportion of older population aged over 65 years is growing rapidly in most countries. In 2035 one third of the Europeans will be over 65 years old (Ambient Assisted Living Joint Programme, 2008; Communication from the Commission to the European Parliament 2010; COOP- 005935-HEBE, 2006). People over age 65 in the United States are expected to hit 70 million by 2030. Statistics show that about one third of home-dwelling older people fall each year (Tinetti, et al., 1988). Falls are the leading cause of deaths by injury for the older population. People who have fall injuries suffer moderate to severe injuries, such as, lacerations, soft tissue injuries, hip fractures, or head traumas. These injuries can make it difficult for those to get around, live independently, and can increase their risk of an early death. Besides physical injuries, falls may have other negative outcomes through resulting in or increasing fear of falling that affects the quality of life among older people. Also, these outcomes force older people to live bedridden together with threatening their independent life and restricting their mobility and social activities (Suzuki, et al., 2002; Yardley & Smith 2002).

Older people are afraid of remain lying and being unable to get up after falling (Melander-Wikman, et al., 2007), and in reality, around half of fallers were not able to get up by themselves or summon help after the fall (Bueno-Cavanillas, et al., 2000). On average, fallers lie helplessly for more than 10 minutes after a fall, and in 3% of non-injurious fall cases the faller had been waiting for more than one hour before getting help (Tinetti, et al., 1993). Lying in long period can increase duration and cost of hospitalisation, institutionalisation and high morbidity-mortality rate (Gurley, et al., 1996; Tinetti, et al., 1993).

Many fall detection systems have been developed to support independence and safety of older people (Brownsell & Hawley, 2004; Melander-Wikman, et al., 2007).

To prevent long lies commercially available personal emergency response systems (PERS) provide applications to call for help. However, in the case of an emergency, the person may be unable or unwilling to activate the PERS alarm. According to some reports, around 80% of older people wearing PERS and being unable to get up after a fall did not use their alarm system to call for help (Fleming, et al., 2008a; Heinbüchner, et al., 2010). In such cases an automatic fall detector could detect a fall and call for help automatically. Hence, a highly accurate fall detection system is an important setting.

Some commercially available automatic fall detection systems exist, typically applying accelerometer based detection methods and attachment sites at the waist or wrist as summarized by Noury, et al., (2008). However, most fall detection applications in the literature are prototypes or applications for research purposes (Bourke, et al., 2007a; Diaz, et al., 2004; Karantonis, et al., 2006; Lindemann, et al., 2005; Mathie, et al., 2004a; Yoshida, et al., 2005). They are usually designed and tested with data collected from intentional falls and activities of daily living from young test persons in a laboratory environment.

Body movements of elderly people may differ from younger people usually. They typically have less control over the speed of their body movements due to reduced muscle strength with old age. Their movements produce higher peak accelerations when performing certain ADL (Activities Daily Living). This situation leads to increased false positives. If ADL-based measurements can be performed using elderly subjects, robustness of the test methodology would increase. As a result, though good fall detection sensitivity and specificity in laboratory settings has been reported, acceptability and usability of these systems in real life is still scant or missing because of their size and uncomfortable to wear. Other restrictive case for fall detection systems is that self-initiated intentional falls differ from sudden unexpected falls. So far, only few reports exist on data from real-life falls. Thus, real-life data on falls among elderly subjects is important for studying fall mechanism even though it is difficult to ask them.

1.2 Outline of Thesis

Chapter 1 presents an introduction to the project.

Chapter 2 is interested in materials and its features of the proposed wearable fall detection monitoring system. It also explains obviously how to configure these devices.

Chapter 3 gives information about hardware and software implementation of the proposed wearable fall detection monitoring system. In hardware implementation section, OrCAD schematic and layout procedures of the system are given shortly. In software implementation section, mbed Compiler, I^2C serial communication protocol and asynchronous serial communication protocol (UART) are explained step by step. These serial communication protocols are used to transfer data between microcontroller unit and other devices such as accelerometer, gyroscope, GPS module and Bluetooth.

In chapter 4, fall detection algorithm parameters are illustrated step by step. These are threshold based analysis for acceleration magnitude and angular velocity, vertical velocity estimate analysis and body posture analysis. Also, four phases of fall event are described in detail. In addition, the proposed fall detection algorithm of wearable fall detection monitoring system is explained step by step.

In chapter 5, gained data of fall detection parameters from test results are given and these data give information about sensitivity, specificity and accuracy of the proposed wearable fall detection monitoring system. Also, test results are evaluated to approach the best fall detection.

In Chapter 6, conclusion and future works are presented.

CHAPTER TWO
MATERIALS AND ITS FEATURES

2.1 Accelerometer

2.1.1 General Description

In this study, ADXL345 3-axis accelerometer has been chosen because of features such as measurement range (±2-*g*, ±4-*g*, ±8-*g*, or ±16-*g*), high resolution (13-bit), fixed 3.9-m*g*/LSB sensitivity, ultralow power (25 µA to 130 µA), small size (3-mm × 5-mm × 1-mm, 14-lead, plastic package), standard I^2C and SPI serial digital interfacing, 32-level FIFO storage, user convenient and flexible solutions. A variety of built-in features, including motion-status detection and flexible interrupts, greatly simplify implementation of the algorithm for fall detection. This combination of features makes the ADXL345 an ideal accelerometer for fall-detector applications. Figure 2.1 shows the system block diagram and pin definitions of the ADXL345.

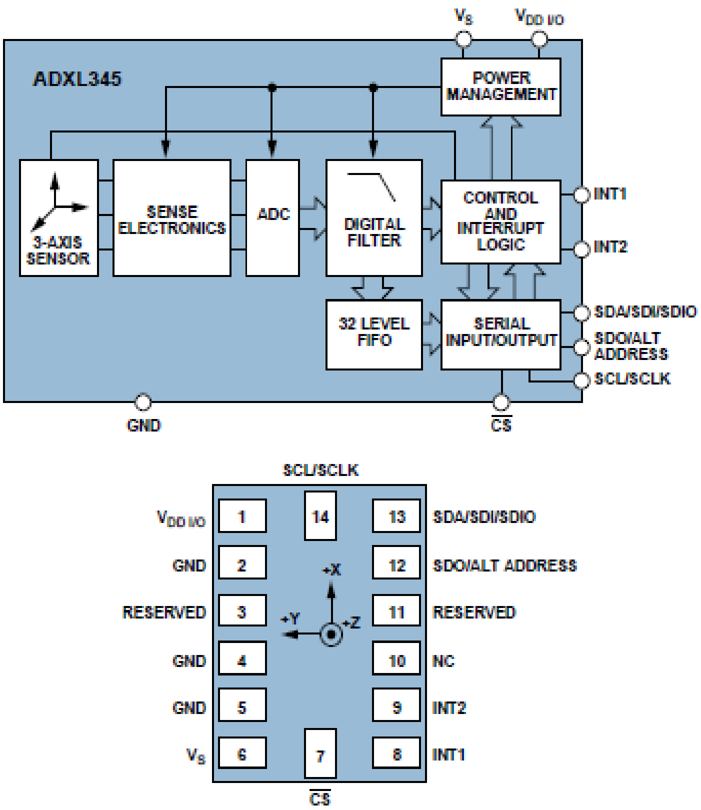

Figure 2.1 ADXL345 system block diagram and pin designations (Jia, 2009)

2.1.2 Communication Interface

ADXL345 communication is done via either I^2C or SPI (3- or 4-wire mode). In this study, I^2C is enabled. Figure 2.2 shows the recommended electrical connection for I^2C mode. The 7-bit I^2C address for the device is 0x53, followed by the R/W bit. The user can select an alternate I^2C address by connecting the SDO/ALT ADDRESS pin to the VDD I/O pin. The 7-bit I^2C address for that configuration is 0x1D, followed by the R/W bit. It supports standard (100 kHz) and fast (400 kHz) data transfer modes if the bus parameters given in and are met. Single- or multiple-byte reads/writes are supported. There are no internal pull-up or pull-down resistors for any unused pins; therefore, there is no known state or default state for the CS or ALT ADDRESS pin if left floating or unconnected. It is required that the CS pin be connected to VDD I/O and that the ALT ADDRESS pin be connected to either VDD I/O or GND when using I^2C.

Sometimes it is important to confirm the validity of a communication sequence before going to the next design stage. This can be done by reading the DEVID register (Address 0x00). It is a read only register that contains 0xE5. If the data read from DEVID is not 0xE5, it is the indication that either the physical connection or command sequence is incorrect.

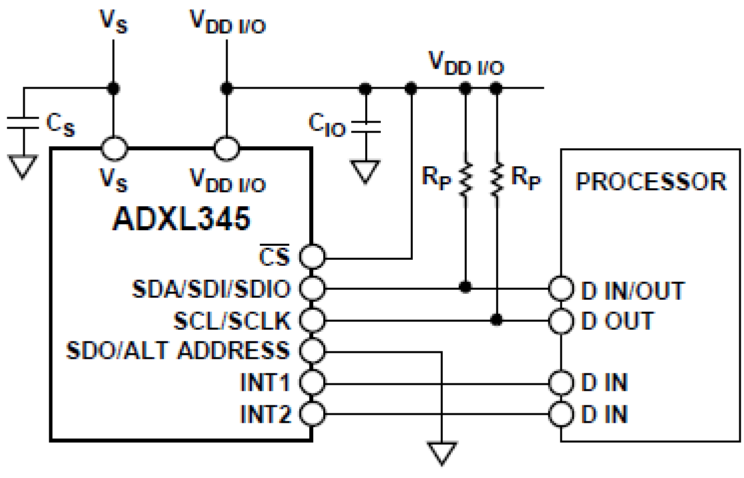

Figure 2.2 Recommended connections for I^2C mode (Tusuzki, n.d.)

2.1.3 Reading Output Data

The DATA_READY interrupt signal indicates that 3-axis of acceleration data is updated in the data registers. It is latched high when new data is ready. Data is read from the DATAX0, DATAX1, DATAY0, DATAY1, DATAZ0, and DATAZ1 registers. To ensure data coherency, multi byte reads have been performed to retrieve data from the ADXL345.

The data format of the ADXL345 is 16 bits. Once acceleration data is acquired from data registers, the user must reconstruct the data. DATAX0 is the low byte register for x-axis acceleration and DATAX1 is the high byte register. In this study, 13-bit resolution has been configured using DATA_FORMAT register. In 13-bit mode, the upper 4 bits are sign bits shown in Figure 2.3. DATA_FORMAT register can also be used for setting other data formats. The ADXL345 uses twos complement data format. When in 13-bit mode, 1 LSB represents about 3.9 m*g*.

D15	D14	D13	D12	D11	D10	D9	D8	D7	D6	D5	D4	D3	D2	D1	D0
SIGN	SIGN	SIGN	SIGN	D11	D10	D9	D8	D7	D6	D5	D4	D3	D2	D1	D0
DATAX1 DATAY1 DATAZ1								DATAX0 DATAY0 DATAZ0							

Figure 2.3 Data construction (Tusuzki, n.d.)

2.1.4 Initialization

Figure 2.4 shows the initialization sequence. A value of 0x0B in the DATA_FORMAT register sets the device to full resolution (13 bits), ±16-*g* measurement range and right justified mode. The reason for the selection of ±16-*g* is the fact that amplitude of acceleration sometimes reaches around 10*g* during a fall. A value of 0x0D in the BW_RATE register selects the device bandwidth and output data rate. An output data rate should be selected that is appropriate for the communication protocol and frequency selected. In this study, I^2C communication protocol has been selected with fast (400 kHz) data transfer mode. Due to communication speed limitations the maximum output data rate when using 400 kHz I^2C is 800 Hz. The 800 Hz output data rate can be used only for communication speeds greater than or equal to 400 kHz so 800 Hz output data rate has been chosen. A setting of 0 in the measure bit of POWER_CTL register places the device into standby mode and a setting of 1 (0x08) places the device into measurement mode.

In a no-turn or single-point calibration scheme, the device has been oriented such that z-axis is in the 1 *g* field of gravity and the other axes, typically the x- and y-axis, are in a 0 *g* field. The output acceleration values have been measured by taking the average of a series of samples. The number of samples has been configured to 128. These values have been stored as calibration values which X_{0g}, Y_{0g}, and Z_{+1g} for the 0*g* measurements on the x- and y-axis and the 1*g* measurement on the z-axis, respectively. Actual acceleration values are obtained by subtracting those values from the measurement values of the accelerometer. In this study, offset registers which can automatically compensate the output, have not been used.

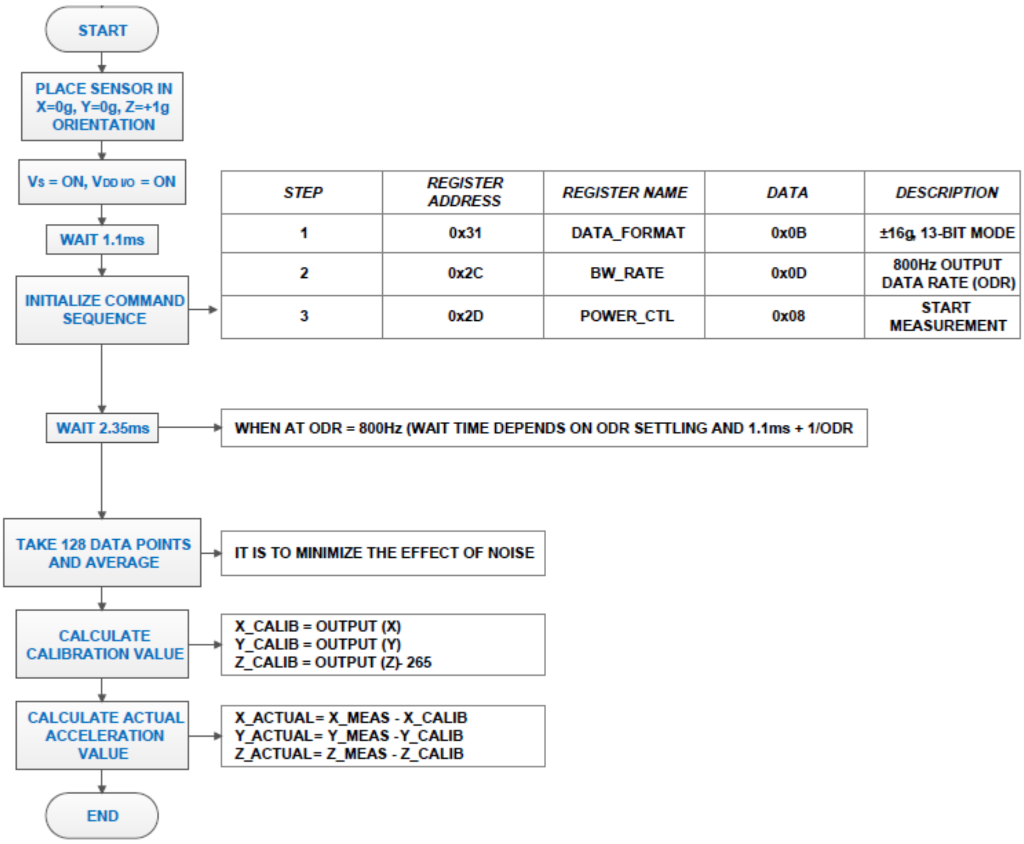

Figure 2.4 Initialization sequence

2.2 Gyroscope

2.2.1 General Description

In this study, ITG-3200 3-axis gyroscope has been chosen because of features such as measurement range (±2000°/sec), high resolution (16-bit), 14.375 LSBs per °/sec sensitivity, low operating current consumption (6.5mA), small size (4-mm × 4-mm × 0.9-mm, 24-pin, QFN package), fast mode I^2C (400kHz) digital interfacing, digitally programmable low pass filter, user convenient and flexible solutions. The ITG-3200 consists of three independent vibratory MEMS gyroscopes, which detect rotational rate about the X (roll), Y (pitch) and Z (yaw) axes. This combination of features makes the ITG-3200 an ideal gyroscope for fall-detector applications. Figure 2.5 shows the system block diagram and pin definitions of the ITG-3200.

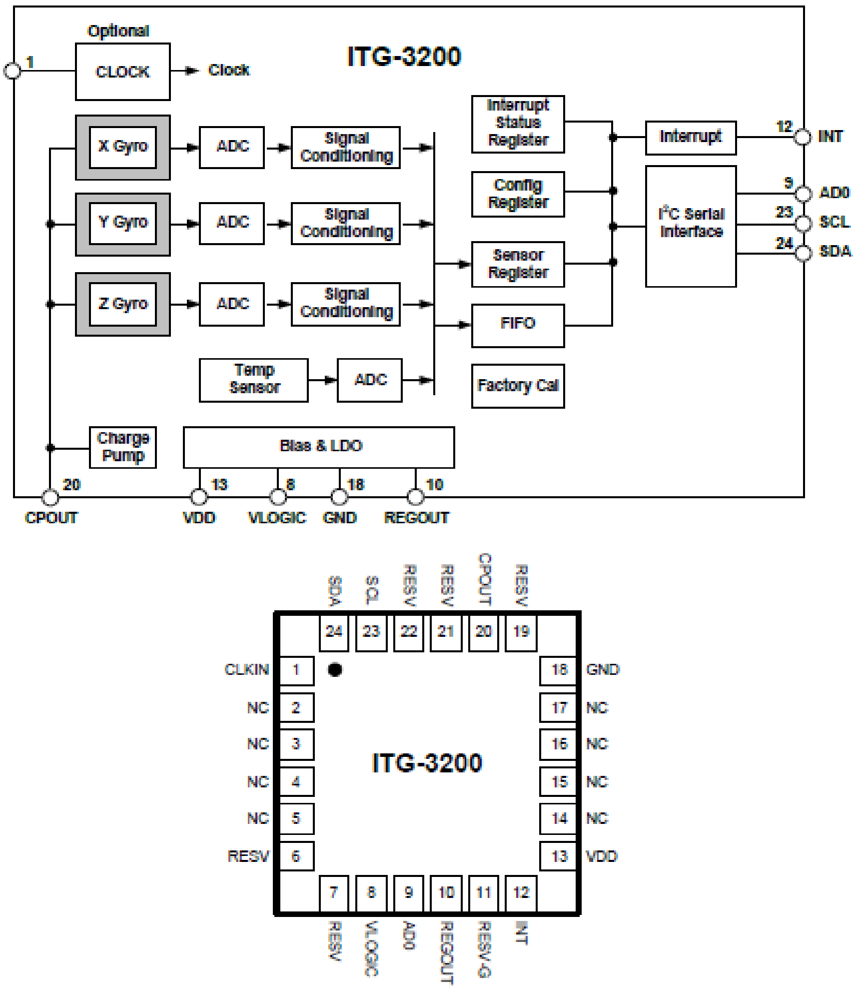

Figure 2.5 ITG-3200 system block diagram and pin designations (InvenSense Inc., 2010)

2.2.2 Communication Interface

The ITG-3200 communicates to a system processor using the I^2C serial interface, and the device always acts as a slave when communicating to the system processor. The logic level for communications to the master is set by the voltage on the VLOGIC pin. SDA and SCL lines typically need pull-up resistors to VDD. The maximum bus speed is 400 kHz.

The slave address of the ITG-3200 devices is b110100X which is 7 bits long. The LSB bit of the 7 bit address is determined by the logic level on pin 9 (AD0). This allows two ITG-3200 devices to be connected to the same I^2C bus. When used in this configuration, the address of the one of the devices should be b1101000 (0x68) when pin 9 is logic low and the address of the other should be b1101001 (0x69) when pin 9 is logic high. The I^2C address is stored in register 0 (WHO_AM_I register).

2.2.3 Reading Output Data

The sensor data registers contain the latest gyro data. They are read-only registers, and are accessed via the serial interface. Data is read from GYRO_XOUT_H, GYRO_XOUT_L, GYRO_YOUT_H, GYRO_YOUT_L, GYRO_ZOUT_H and GYRO_ZOUT_L registers. GYRO_XOUT_L is the low byte register for x-axis gyro data and GYRO_XOUT_H is the high byte register. The RAW_DATA_RDY interrupt signal may be used to determine when new data is ready. To ensure data coherency, multi byte reads have been performed to retrieve data from the ITG-3200. Data format of the ITG-3200 is 16 bits and it uses twos complement data format.

2.2.4 Initialization

Figure 2.6 shows the initialization sequence. A value of 0x18 in the DLPF_FS register sets the device to full scale range (±2000°/sec) and digital low pass filter configuration. It also determines the internal sample rate used by the device. The reason for the selection of ±2000°/sec is the fact that amplitude of angular velocity sometimes reaches around ±500-600°/sec during a fall. A setting of 0 in the DLPF_CFG bits of DLPF_FS register sets the device to low pass filter bandwidth (256Hz) and internal sample rate (8kHz). SMPLRT_DIV register determines the sample rate of the ITG-3200 gyros. A value of 0x09 in the SMPLRT_DIV register sets sample rate divider to 9. The sample rate is given by the following formula:

$$F_{sample} = F_{internal} / (divider+1), \text{ where } F_{internal} \text{ is 8 kHz} \quad (2.1)$$

$$F_{sample} = 8 \text{ kHz} / (9 + 1) = 800\text{Hz, or 1.25ms per sample} \quad (2.2)$$

The output gyro values have been measured by taking the average of a series of samples for device calibration. The number of samples has been configured to 128. These values have been stored as calibration values. Actual gyro values are obtained by subtracting those values from the measurement values of the gyroscope.

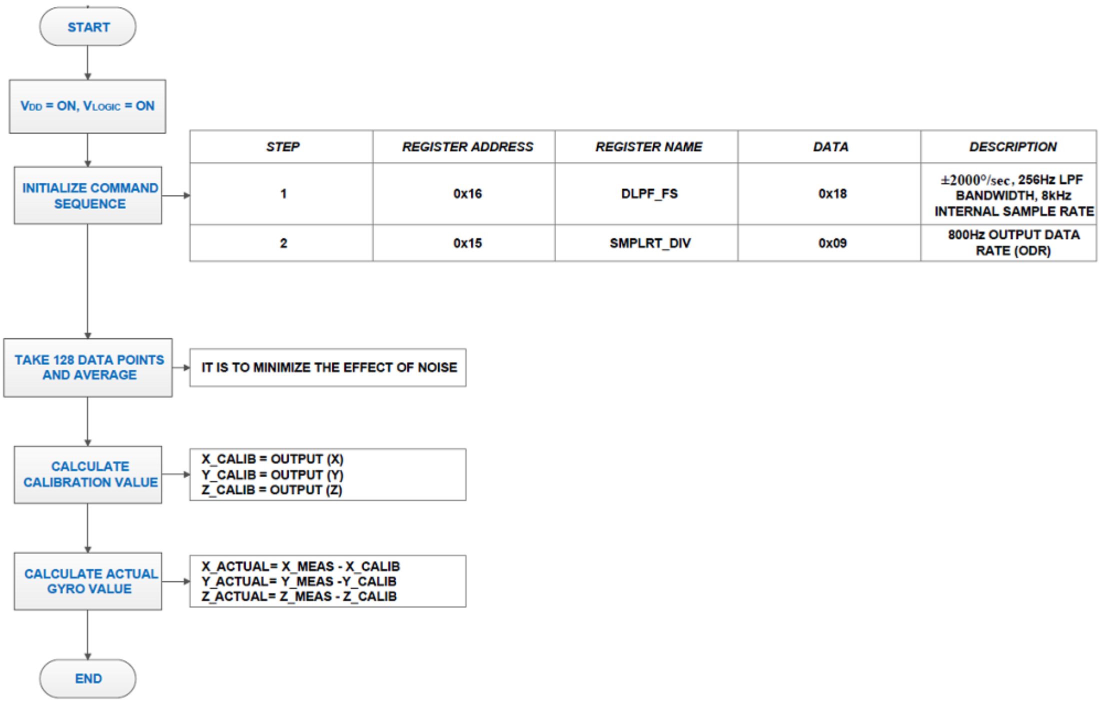

Figure 2.6 Initialization sequence

2.3 Bluetooth

2.3.1 General Description

In this study, JY-MCU Bluetooth wireless serial port module shown in Figure 2.7 has been chosen for wireless communication because many modern portable devices (laptop computers, mobile phones, GPS, etc.) are easily compatible with Bluetooth technology. This module allows our target device to both send and receive the TTL data via Bluetooth technology without connecting a serial cable to our computer. It's easy to use and completely encapsulated. It also supports RXD/TXD serial communication from 9600 to 115200 bps (bits per second, baud rate). Its size is small (4.4 cm x 1.6 cm x 0.7 cm) and its range is around 10 meters (~33 ft). It is compatible with 3.6-6V power and its current consumption is 40mA max.

Figure 2.7 JY-MCU Bluetooth module (Gökçegöz, 2013)

2.3.2 Configuration

This section describes how to configure some parameters of JY-MCU Bluetooth module such as name and baud rate. The module comes with a default baud rate of 9600, 8 data bits, 1 stop bit & no parity. In order to reconfigure the Bluetooth module TTL serial port and a terminal program such as Putty. In this study, basic 5V Sparkfun FTDI breakout board has been used as a USB to serial port converter to configure the module. Bluetooth module has been connected to FTDI board as in the Figure 2.8. After opening terminal program Putty, the module has been connected with default setting 9600 baud rate, 8 data bits, 1 stop bit & no parity.

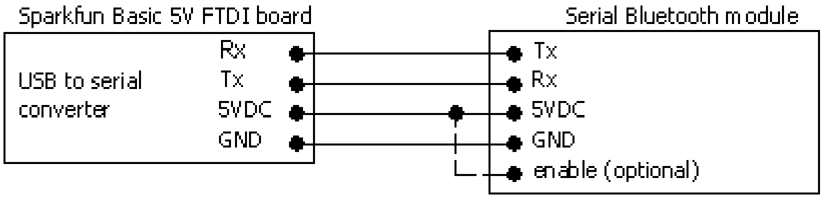

Figure 2.8 Module configuration connections

The module is configurable through AT commands shown in Table 2.1 such as AT+VERSION, AT+BAUDx. Firstly, you should type AT in Putty and if the response is OK means that everything is correct. The module has been set with the command AT+BAUD8 and it has been configured to work on a serial speed of 115200 baud rate.

Table 2.1 AT commands

Command	**Description**	**Options**	**Response**
AT+VERSION	Returns the software version of the module		OKJY-MCUV1.5
AT+BAUDx	Sets the baud rate of the module. The command AT+BAUD8 sets the baud rate to 115200	1>>1200 2>>2400 3>>4800 4>>9600(Default) 5>>19200 6>>38400 7>>57600 8>>115200	OK115200
AT+NAMEOpenPilot	Sets the name of the module	Any name can be specified up to 20 characters	OKsetname
AT+PINxxxx	Sets the pairing password of the device	Any 4 digit number can be used, the default pin code is 1234	OKsetPIN
AT+PN	Sets the parity of the module	AT+PN>>No parity check	OK None

2.4 Global Positioning System (GPS)

2.4.1 General Description

In this study, GPS receiver engine board EM-406A shown in Figure 2.9 has been chosen to determine latitude and longitude information of faller. The module makes it possible to detect the geographical coordinates of the faller and the place where the faller is (street, etc.). Only disadvantage of GPS chip is to provide localization outside the home. It also supports RX/TX serial communication with 4800 bps (bits per second, baud rate). Its dimension is 30 mm x 30 mm x 10.5 mm and its accuracy of position is around 10 meters. It is compatible with 4.5-6.5V power and its current consumption is 44mA max.

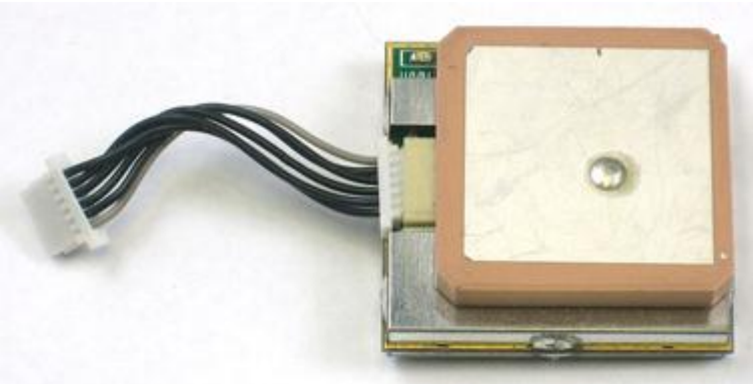

Figure 2.9 EM-406A GPS receiver engine board (GlobalSat Technology Corporation, n.d.)

2.4.2 Features

This section describes features of EM-406A GPS receiver engine board in detail.

- SiRF Star III high performance GPS Chipset
- Very high sensitivity (Tracking Sensitivity: -159dBm)
- Extremely fast TTFF (Time To First Fix) at low signal level
- Support NMEA 0183 data protocol
- Built-in SuperCap to reserve system data for rapid satellite acquisition
- Built-in patch antenna

- LED indicator for GPS fix or not fix
  LED OFF: Receiver switch off
  LED ON: No fixed, Signal searching
  LED Flashing: Position Fixed
- WAAS ENGOS is supported.

2.5 Vodafone Vodem K3770

2.5.1 General Description

The Vodafone K3770 vodem shown in Figure 2.10 allows you to connect your mbed microcontroller to the internet from any location in the world. In this study, it is used to send SMS for informing victim's family. When elderly people perform fall event maybe it is emergency situation, K3770 vodem makes it possible to inform victim's family immediately by sending SMS.

Figure 2.10 Vodafone vodem K3770 (Vodafone, n.d.)

2.6 Microcontroller Unit

2.6.1 General Description

In this study, mbed NXP LPC1768 prototyping board shown in Figure 2.11 has been chosen because of available features such as works with the groundbreaking mbed tool suite, easy to explore designs quickly so you can be adventurous, more inventive, and more productive. The mbed NXP LPC1768 prototyping board allows you to create designs without having to work with low-level microcontroller details, so you can develop your designs faster than ever. Also, designers compose and compile embedded software using a browser-based IDE, then download it quickly and easily, using a simple drag-and-drop function, to the board's NXP Cortex-M3 microcontroller LPC1768.

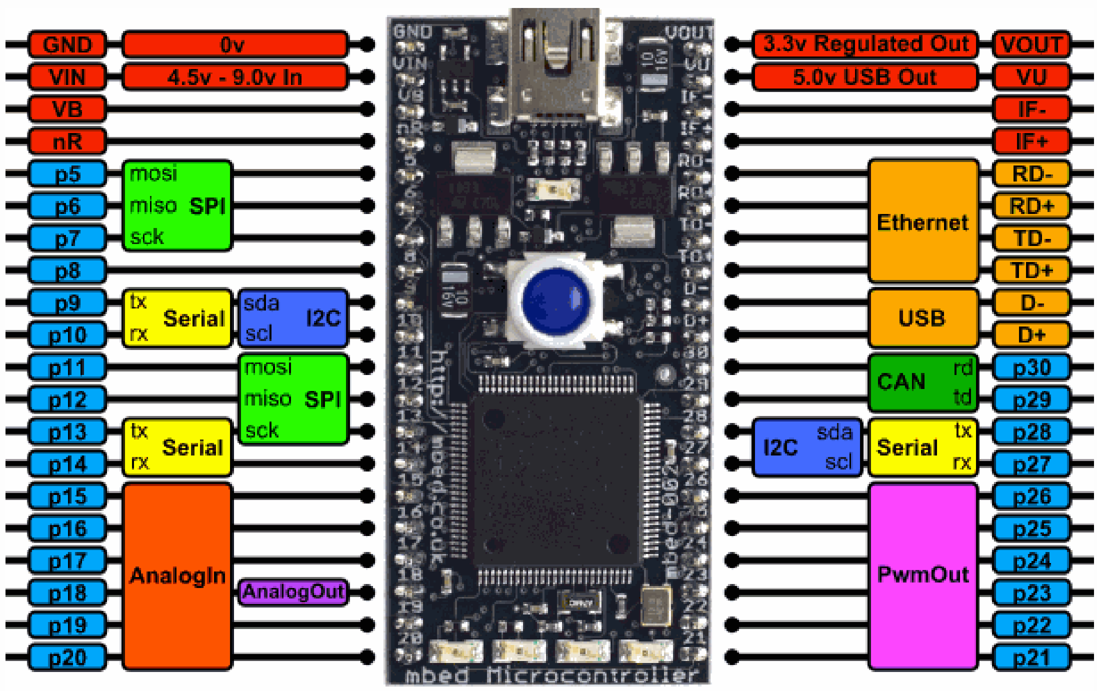

Figure 2.11 mbed NXP LPC1768 prototyping board (NXP, 2009)

2.6.2 Features & Benefits

2.6.2.1 Features

- Convenient form-factor: 40-pin DIP, 0.1-inch pitch
- Drag-and-drop programming, with the board represented as a USB drive

- Best-in-class Cortex-M3 hardware
    - 100 MHz ARM with 64 KB of SRAM, 512 KB of Flash
    - Ethernet, USB OTG
    - SPI, I2C, UART, CAN
    - GPIO, PWM, ADC, DAC
- Easy-to-use online tools
    - Web-based C/C++ programming environment
    - Uses the ARM RealView compile engine
    - API-driven development using libraries with intuitive interfaces
    - Comprehensive help and online community

2.6.2.2 Benefits

- Get started right away, with nothing to install
- Get working fast, using high-level APIs
- Explore, test, and demonstrate ideas more effectively
- Write clean, compact code that's easy to modify
- Log in from anywhere, on Windows, Mac or Linux

2.6.3 LPC1768 Microcontrollers

The NXP microcontroller family LPC1768 is a series of cost-effective, low-power Cortex-M3 devices that operate at up to 100MHz. They feature best-in-class peripheral support, including Ethernet, USB 2.0 host/OTG/device, and CAN 2.0B. There are 512 KB of Flash memory and 64 KB of SRAM. Features of NXP LPC1768 microcontroller are given in Table 2.2.

Table 2.2 Features of NXP LPC1768 microcontroller

LPC1768	
Arm Cortex M3 Core	• 100 MHz operation • Memory protection unit • Four power mode: sleep, deep sleep, power down, and deep power down
Memories	• 512 KB of flash memory • 64 KB of SRAM
Serial Peripherals	• 10/100 Ethernet MAC • USB 2.0 full-speed device/Host /OTG controller with on-chip PHY • Four UARTs with fractional baud rate generation • Two CAN 2.0B controllers • Three SSP/SPI controllers • Three I2C-bus interfaces with one supporting Fast Mode Plus (1-Mbit/s data rates) • I2S interface for digital audio
Analog Peripherals	• 12 bit ADC with 8 channels • 10 bit DAC
Other Peripherals	• Ultra low power (< 1µA) RTC • Four 32-bit general purpose timers
Package	• 100-pin LQFP (14 x 14 x 1.4mm)

2.7 Peripherals

2.7.1 Buzzer

CEM-1203(42) magnetic buzzer shown in Figure 2.12 has been used to send out alarm sound to the faller. When the fall detection algorithm decides that a fall event occurs, microcontroller unit (MCU) will activate the buzzer. Also, the buzzer makes it possible to cancel the false alarm by providing auditory feedback to the blind person when a fall doesn't occur. In other words, if users of the developed wearable fall detection monitoring system hear false alarm, they can deactivate the system by pressing a button in order not to alert emergency service call.

Figure 2.12 CEM-1203(42) magnetic buzzer (CUI Inc, 2006)

The buzzer's rated voltage is 3.5V and its frequency is 2048Hz. To trigger buzzer, pulse width modulation (PWM) technique shown in Figure 2.13 is used. Pulse width modulation (PWM) is a simple method of using a rectangular digital waveform to control an analog variable. The PwmOut interface on the mbed NXP LPC1768 microcontroller is used to control the frequency and mark-space ratio of a digital pulse train. The magnetic buzzer is connected to one of the PWM outputs on the microcontroller and its duty cycle is set to %50 and frequency to 2048Hz. The duty cycle formula is given in Equation 2.3.

Duty cycle = 100% * (pulse on time) / (pulse period) (2.3)

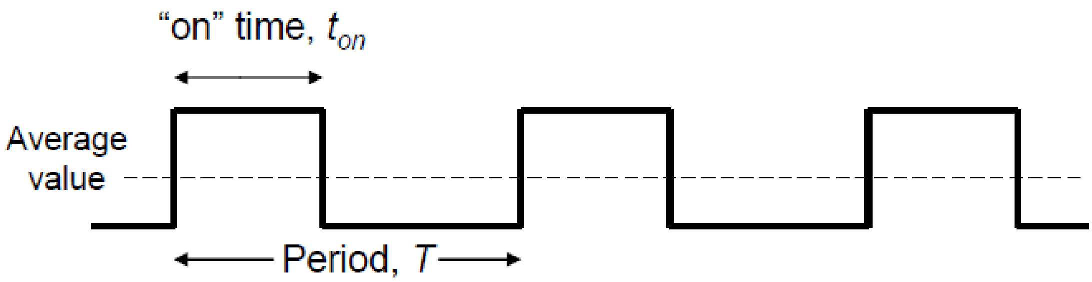

Figure 2.13 Pulse width modulation (PWM) technique (Toulson, & Wilmshurst, 2012)

2.7.2 Button

Two push buttons shown in Figure 2.14 have been used to control the proposed wearable fall detection monitoring system. One of them is used to activate local file system which accesses the local mbed microcontroller USB disk drive. The push button is connected by connecting ground to interrupt input pin (p8 in our code) and has an internal pull up resistor. When interrupt input pin changes by pressing button, software of monitoring system starts to record our accelerometer and gyro data on the local file system. In other words, it makes it possible to record accelerometer and gyro output data to the flash specific part that is connected to the interface chip. Also, this button can be used to deactivate system when false alarm occurs. Other push button on the mbed NXP LPC1768 prototyping board is used to reset all system.

Figure 2.14 Push button

2.7.3 Led

Four leds on the mbed NXP LPC1768 prototyping board can be used to indicate that a fall event occurs or not. Microcontroller unit (MCU) may trigger to turn on leds by providing visual feedback to the faller who may be deaf person. Deaf person cannot be able to hear alarm sound of buzzer. This design gives deaf person a chance to deactivate system by pressing button when false alarm occurs.

2.7.4 Battery

Two lithium polymer 3.7V shown in Figure 2.15, 1500mAh batteries connected series (7.4V) have been used to power the proposed wearable fall detection monitoring system. The battery has been chosen because of features such as its voltage is compatible with mbed NXP LPC1768 prototyping board (4.5-9V input voltage), long battery life, rechargeable and economic.

Figure 2.15 Li-Po battery

2.7.5 Housing

To perform actual fall detection algorithm testing and data collection, robust housing solution has been chosen. To house our devices such as accelerometer, gyroscope, microcontroller unit and remaining all peripherals, plastic box with a rectangular shape has been used. All peripherals of wearable fall detection monitoring system have been mounted on printed circuit board (PCB). The PCB is attached to the plastic box shown in Figure 2.16 with screw.

Figure 2.16 Housing

CHAPTER THREE

SYSTEM DESIGN

3.1 Hardware Implementation

The wearable fall detection monitoring system consists of seven parts, including accelerometer, gyroscope, Bluetooth, GPS module, Vodafone vodem, microcontroller unit and buzzer & led & battery & button. A block diagram of the system is shown in Figure 3.1.

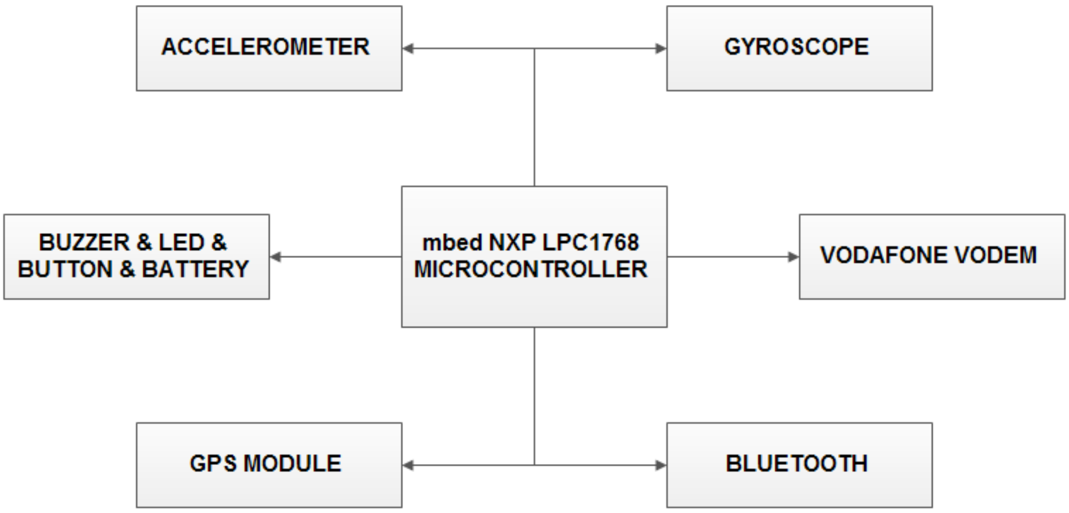

Figure 3.1 Block diagram of the system

3.1.1 OrCAD

3.1.1.1 Schematic

OrCAD is a suitable of tools from Cadence for the design and layout of printed circuit boards (PCBs). In this study, version 9.2 of the OrCAD has been used for designing an entire circuit board from start to finish. OrCAD consists of two tools. OrCAD Capture is used for design entry in schematic form. Capture is used to draw the schematic diagram of wearable fall detection monitoring system. OrCAD Layout is a tool for designing the physical layout of components and circuits on a PCB.

Layout is used for the actual layout design of the PCB. To draw schematic diagram of wearable fall detection monitoring system, following steps must be performed:

- Starting a New Schematic Project
- Creating a Schematic Parts Library
- Creating Schematic Symbols
- Schematic Entry
    - Setting up the Environment
    - Placing Parts & Making Connections

3.1.1.2 Steps to Export Design to Layout

After completing schematic diagram of the system, several steps must be performed to export the design to Layout:

- Annotation
- Intersheet References
- Creating Footprint Libraries: Footprints are a representation of the physical area that a part occupies on a PCB. A footprint is a set of copper pads that corresponds directly to the component leads. This step is one of the most crucial steps to the design of the PCB. Any mix-up in a footprint will ruin entire design. Therefore extra-special care must be taken when matching a footprint to the corresponding component. Library of footprints are created to begin working in layout to proceed with the design.

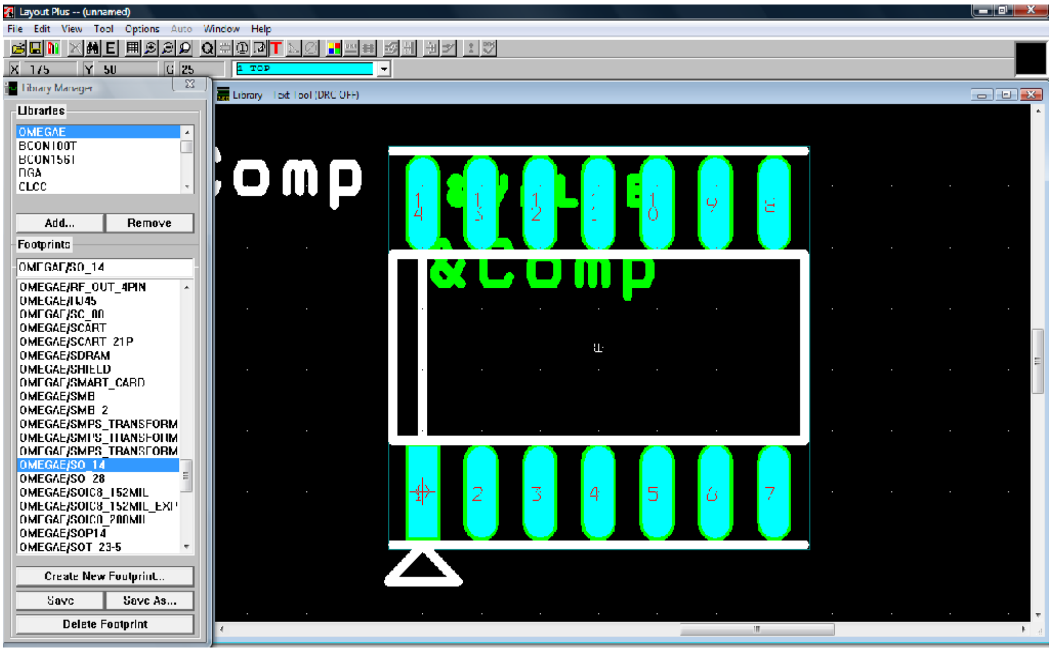

Figure 3.2 Library manager for example footprint

As with the schematic symbols, be very careful to check that these footprints for correctness before using them. OrCAD has many existing footprints that you can use in your own design shown in Figure 3.2. In this study, footprints have been created for parts that don't already have one. Most datasheets for parts contain the mechanical information necessary to make a correct footprint.

- Assigning Footprints to Parts
- Creating the Netlist: To export the design to Layout, you must first create a netlist. A netlist is a file that has all the parts, footprints and nets for the design in a format that can be read by the layout program.

3.1.1.3 Layout

After exporting the design to Layout, importing the design in Layout is needed. To route Layout of wearable fall detection monitoring system, following steps must be performed:

- Creating a New Board
- Getting Around & Placing Parts
- Routing Power, Ground and Copper Pours

- Routing Other Nets
- Checking For Errors
- Cleaning Up & The Design
- Documenting the Design: Good documentation of your design will help both in manufacturing and debug.
- Creating Gerber Files: After finishing the design and everything is ready to send off the Gerber Files for fabrication.
- Viewing the Gerber Files: Before submitting the Gerber files for fabrication, it is best to look at them in a Gerber viewer. OrCAD has a built in Gerber viewer and editor called GerbTool. GerbTool is used to catch mistakes there that you don't see in Layout.

PCB of the design consists of 2 layers. The top and bottom layers are used for routing nets between parts shown in Figure 3.3 and Figure 3.4 and placement of parts shown in Figure 3.5. To send off the design for fabrication, Gerber files of following layers are needed:

- TOP: Layer 1 – Top Routing
- BOT: Layer 2 – Bottom Routing
- SMT: Top Layer Solder mask
- SMB: Bottom Layer Solder mask
- SST: Top Layer Silk Screen
- DRD: Drill
- FAB: Fabrication Drawing

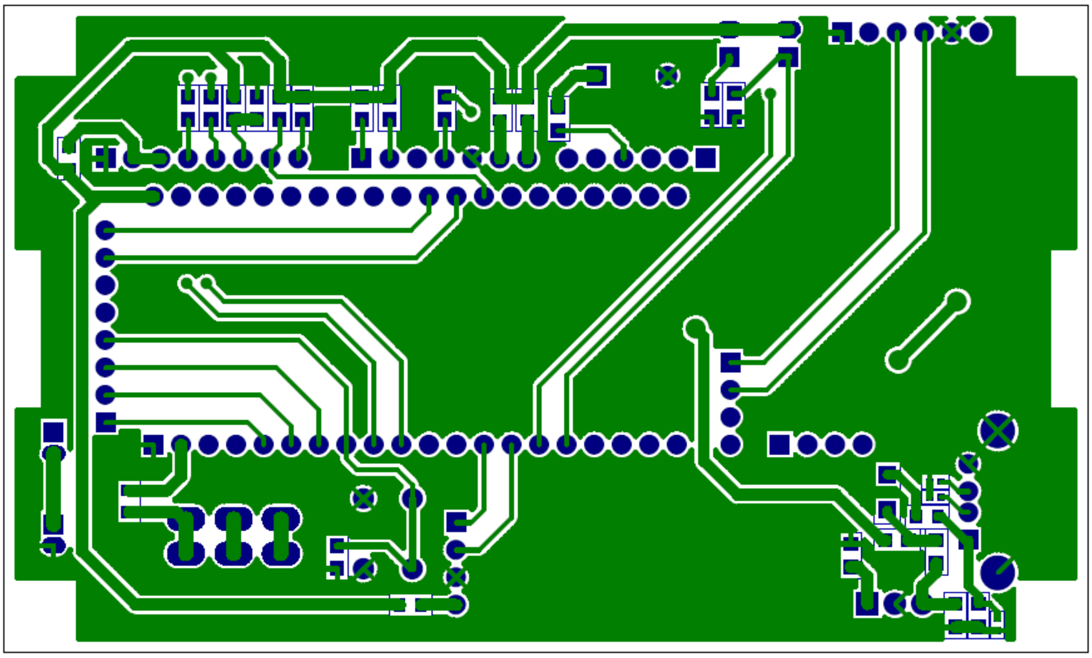

Figure 3.3 Top layer routing of the PCB

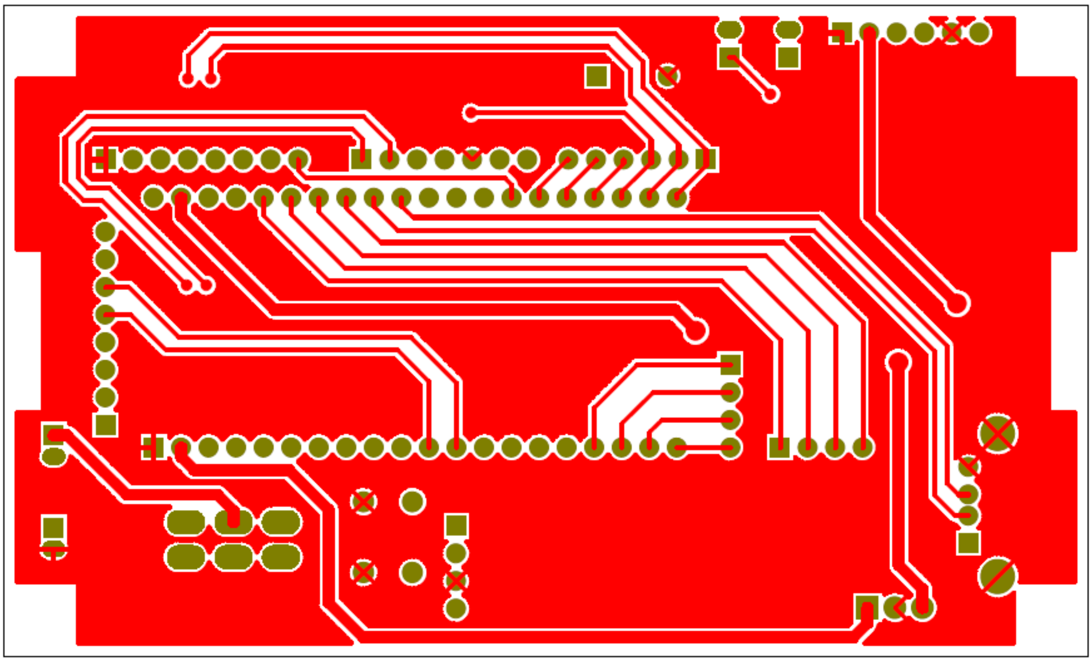

Figure 3.4 Bottom layer routing of the PCB

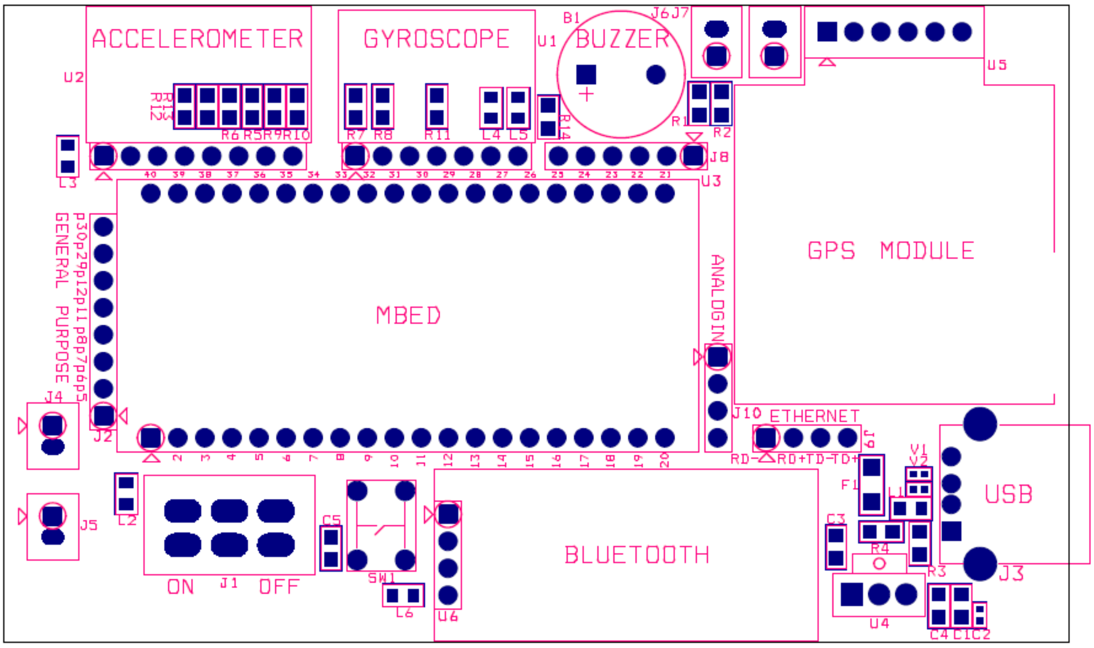

Figure 3.5 Placement of parts on the PCB

3.2 Software Implementation

In this study, mbed Compiler has been used to design software of wearable fall detection monitoring system. The mbed Compiler allows you write programs in C++ and then compile and download them to run on the mbed NXP LPC1768 microcontroller. All programs in this study have been written in C++ language. There's no need to run an install or setup program, since the compiler runs online. The mbed Compiler is shown in Figure 3.6.

In this section, description of serial communication protocols (I^2C, UART) which are used to communicate between MCU (Microcontroller Unit) and other devices (GPS module, Accelerometer, Gyroscope, Bluetooth) is given briefly. I^2C communication protocol has been used to transfer data between MCU and other devices such as accelerometer, gyroscope. RX/TX asynchronous serial communication protocol (UART) has been used to transfer data between MCU and other devices such as Bluetooth, GPS module. Software design of fall detection algorithm will be given detailed in next chapter.

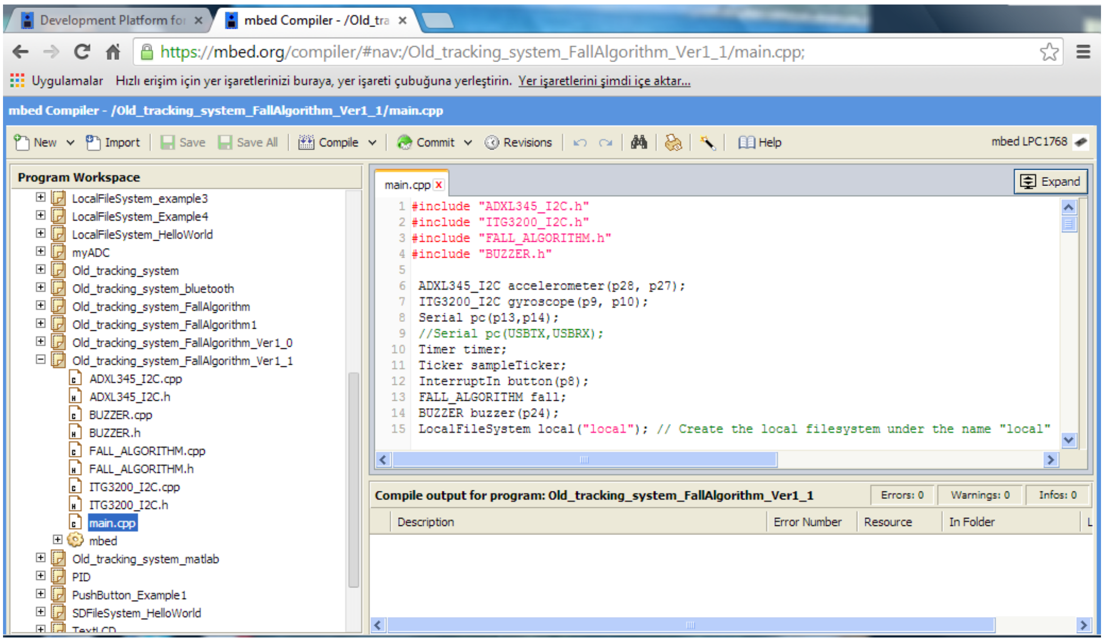

Figure 3.6 mbed compiler

Serial interfaces stream their data, one single bit at a time. These interfaces can operate on as little as one wire, usually never more than four. Each of these serial interfaces can be sorted into one of two groups: synchronous or asynchronous.

A synchronous serial interface always pairs its data line(s) with a clock signal, so all devices on a synchronous serial bus share a common clock. This makes for a more straightforward, often faster serial transfer, but it also requires at least one extra wire between communicating devices. Examples of synchronous interfaces include SPI, and I^2C.

Asynchronous means that data is transferred without support from an external clock signal. This transmission method is perfect for minimizing the required wires and I/O pins, but it does mean we need to put some extra effort into reliably transferring and receiving data. Examples of asynchronous interfaces include UART.

3.2.1 I^2C Interface

I^2C is a two wire interface comprised of the signals serial data (SDA) and serial clock (SCL). In general, the lines are open-drain and bi-directional. In a generalized

I^2C interface implementation, attached devices can be a master or a slave. The master device puts the slave address on the bus, and the slave device with the matching address acknowledges the master.

3.2.1.1 Start (S) and STOP (P) Conditions

Communication on the I^2C bus starts when the master puts the START condition (S) on the bus, which is defined as a HIGH-to-LOW transition of the SDA line while SCL line is HIGH (see Figure 3.7). The bus is considered to be busy until the master puts a STOP condition (P) on the bus, which is defined as a LOW to HIGH transition on the SDA line while SCL is HIGH (see Figure 3.7). Additionally, the bus remains busy if a repeated START (Sr) is generated instead of a STOP condition.

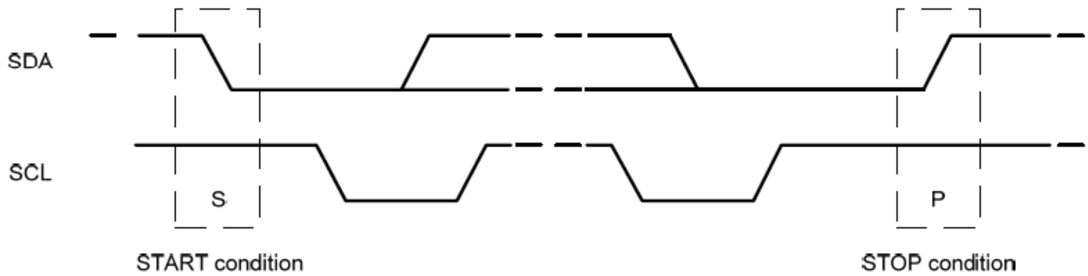

Figure 3.7 START and STOP conditions (InvenSense Inc., 2010)

3.2.1.2 Data Format / Acknowledge

I^2C data bytes are defined to be 8 bits long. There is no restriction to the number of bytes transmitted per data transfer. Each byte transferred must be followed by acknowledge (ACK) signal. The clock for the acknowledge signal is generated by the master, while the receiver generates the actual acknowledge signal by pulling down SDA and holding it low during the HIGH portion of the acknowledge clock pulse.

If a slave is busy and cannot transmit or receive another byte of data until some other task has been performed, it can hold SCL LOW, thus forcing the master into a wait state. Normal data transfer resumes when the slave is ready, and releases the clock line (see Figure 3.8).

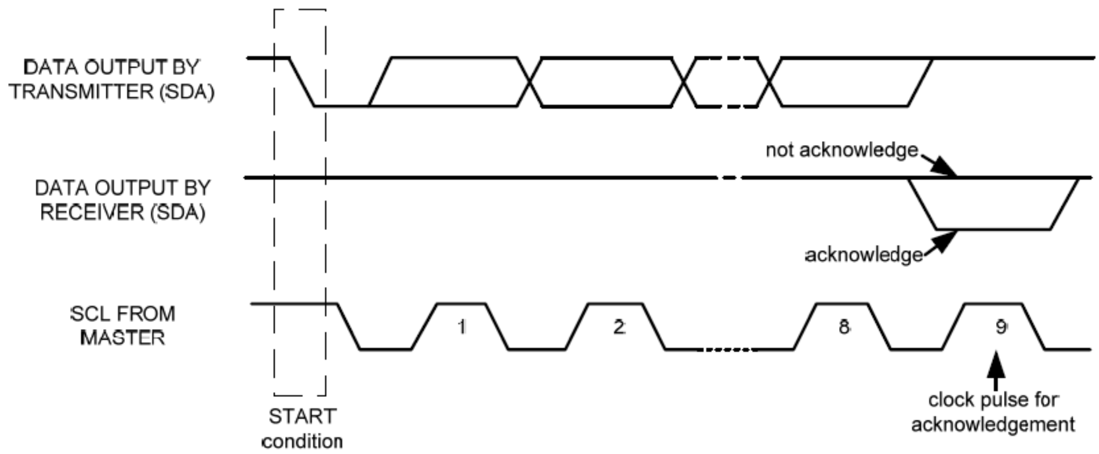

Figure 3.8 Acknowledge on the I^2C bus (InvenSense Inc., 2010)

3.2.1.3 Communications

After starting communications with the START condition (S), the master sends a 7-bit slave address followed by an 8th bit, the read/write bit. The read/write bit indicates whether the master is receiving data from or is writing to the slave device. Then, the master releases the SDA line and waits for the acknowledge signal (ACK) from the slave device. Each byte transferred must be followed by an acknowledge bit. To acknowledge, the slave device pulls the SDA line LOW and keeps it LOW for the high period of the SCL line. Data transmission is always terminated by the master with a STOP condition (P), thus freeing the communications line. However, the master can generate a repeated START condition (Sr), and address another slave without first generating a STOP condition (P). A LOW to HIGH transition on the SDA line while SCL is HIGH defines the stop condition. All SDA changes should take place when SCL is low, with the exception of start and stop conditions (see Figure 3.9).

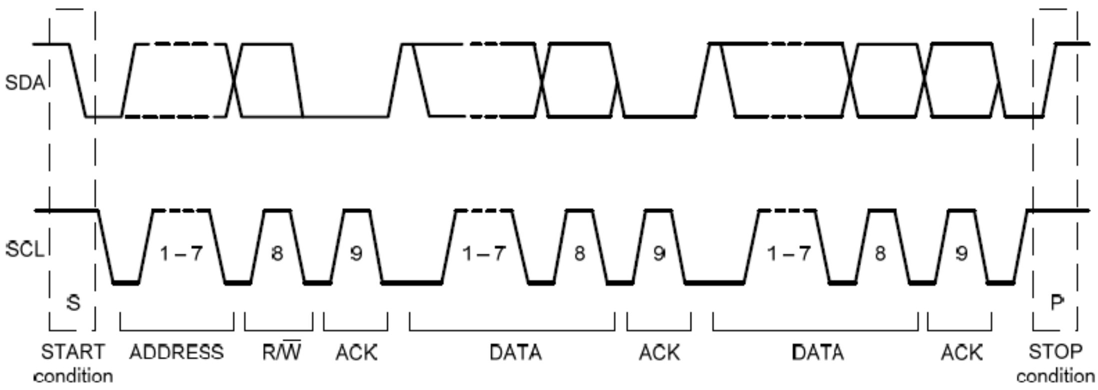

Figure 3.9 Complete I^{2}C data transfer (InvenSense Inc., 2010)

To write our sensor (accelerometer and gyroscope) registers, the master (MCU) transmits the start condition (S), followed by the I^{2}C address and the write bit (0). At the 9th clock cycle (when the clock is high), our sensors acknowledge the transfer. Then the master puts the register address (RA) on the bus. After the sensors acknowledge the reception of the register address, the master puts the register data onto the bus. This is followed by the ACK signal, and data transfer may be concluded by the stop condition (P). To write multiple bytes after the last ACK signal, the master can continue outputting data rather than transmitting a stop signal. In this case, our sensors automatically increment the register address and load the data to the appropriate register. The following Figure 3.10 shows single and two-byte write sequences.

Single-Byte Write Sequence

Master	S	AD+W		RA		DATA		P
Slave			ACK		ACK		ACK	

Burst Write Sequence

Master	S	AD+W		RA		DATA		DATA		P
Slave			ACK		ACK		ACK		ACK	

Figure 3.10 Single-byte and multiple-byte write sequence (InvenSense Inc., 2010)

To read the sensor (accelerometer and gyroscope) registers, the master (MCU) first transmits the start condition (S), followed by the I^{2}C address and the write bit

(0). At the 9th clock cycle (when clock is high), our sensors acknowledge the transfer. The master then writes the register address that is going to be read. Upon receiving the ACK signal from the sensors, the master transmits a start signal followed by the slave address and read bit. As a result, the sensors send an ACK signal and the data. The communication ends with a not acknowledge (NACK) signal and a stop bit from master. The NACK condition is defined such that the SDA line remains high at the 9th clock cycle. To read multiple bytes of data, the master can output an acknowledge signal (ACK) instead of a not acknowledge (NACK) signal. In this case, our sensors automatically increment the register address and output data from the appropriate register. The following Figure 3.11 shows single and two-byte read sequences.

Single-Byte Read Sequence

Master	S	AD+W		RA		S	AD+R			NACK	P
Slave			ACK		ACK			ACK	DATA		

Burst Read Sequence

Master	S	AD+W		RA		S	AD+R			ACK		NACK	P
Slave			ACK		ACK			ACK	DATA		DATA		

Figure 3.11 Single-byte and multiple-byte read sequence (InvenSense Inc., 2010)

3.2.2 Asynchronous Serial Communication Interface

The asynchronous serial protocol has a number of built-in rules - mechanisms that help ensure robust and error-free data transfers. These mechanisms are:

- Data bits,
- Synchronization bits,
- Parity bits,
- Baud rate.

Through the variety of these signaling mechanisms, you’ll find that there’s no one way to send data serially. The protocol is highly configurable. The critical part is making sure that both devices on a serial bus are configured to use the exact same protocols. Each block (usually a byte) of data transmitted is actually sent in a packet or frame of bits. Frames are created by appending synchronization and parity bits to our data.

Figure 3.12 Serial frame, some symbols in the frame have configurable bit sizes (Sparkfun, n.d.)

The baud rate specifies how fast data is sent over a serial line. It's usually expressed in units of bits-per-second (bps). If you invert the baud rate, you can find out just how long it takes to transmit a single bit. This value determines how long the transmitter holds a serial line high/low or at what period the receiving device samples its line.

The real meat of every serial packet is the data it carries. The amount of data in each packet can be set to anything from 5 to 9 bits. Certainly, the standard data size is your basic 8-bit byte, but other sizes have their uses (see Figure 3.12).

The synchronization bits are two or three special bits transferred with each chunk of data. They are the start bit and the stop bit(s). True to their name, these bits mark the beginning and end of a packet. There's always only one start bit, but the number of stop bits is configurable to either one or two (though it's commonly left at one). The start bit is always indicated by an idle data line going from 1 to 0, while the stop bit(s) will transition back to the idle state by holding the line at 1.

Parity is a form of very simple, low-level error checking. It comes in two flavors: odd or even. To produce the parity bit, all 5-9 bits of the data byte are added up, and the evenness of the sum decides whether the bit is set or not.

A serial bus consists of just two wires-one for sending data and another for receiving. As such, serial devices should have two serial pins: the receiver, RX, and the transmitter, TX. A serial interface where both devices may send and receive data is either full-duplex or half-duplex. Full-duplex means both devices can send and receive simultaneously. Half-duplex communication means serial devices must take turns sending and receiving.

CHAPTER FOUR
FALL DETECTION ALGORITHM

4.1 Fall Detection Algorithm Parameters

A fall, including impact, has been defined to have four distinct phases (Noury, et al., 2008b): (1) the pre-fall phase, (2) critical phase or pre-impact phase, (3) post-fall phase and (4) recovery phase.

During the "pre-fall" phase the person performs usual activities of daily living (ADL), with occasional sudden movements, like sitting or lying down rapidly, which must be distinguished from a fall. So, "pre-fall" phase may include some instability because of performing ADL such as walking, running and sitting down.

The "critical phase or pre-impact phase" consists of the sudden free fall-like movement of the body toward the ground, ending with a vertical shock on the ground. The duration of this phase is extremely short ($T_1 - T_0$ = 300–500 ms). During the critical phase of a fall, there is a temporary period of "free fall". During this period, the vertical speed also increases linearly with time because of gravitational acceleration.

During the "post-fall" phase, the person remains inactive, frequently lying on the ground. The "post-fall" phase shouldn't last too long ($T_2 - T_1 < 1$ h) to reduce the consequences of the fall such as high morbidity-mortality rate.

The "recovery" phase is either intentional – the person is able get up and move on his own – or with help from another person.

The fall event is a cascade of phases. Some characteristics of interrupted movement can indicate the incoming fall already some seconds before the actual fall event. The four phases of a fall event is shown in Figure 4.1.

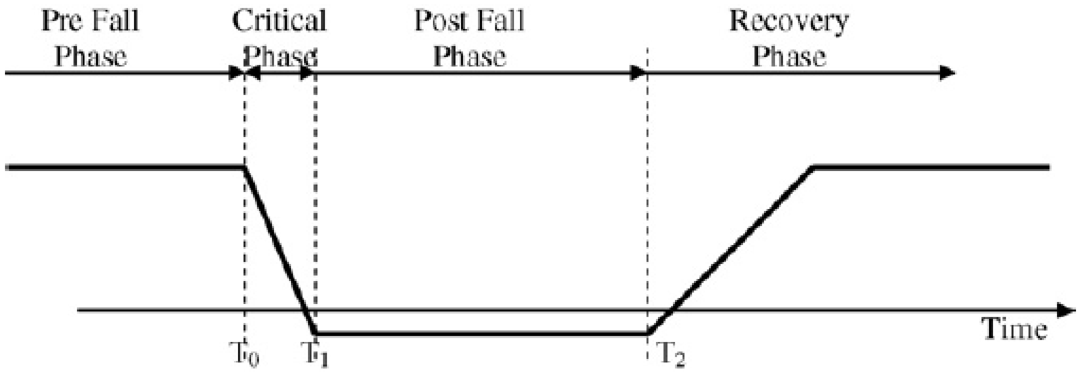

Figure 4.1 The four phases of a fall event (Kangas, 2011)

The proposed fall detection solution can be divided into four steps: threshold-based analysis for acceleration magnitude, vertical velocity estimate analysis, body posture analysis, and threshold based-analysis for angular velocity. The proposed wearable fall detection monitoring system is placed at chest of a person because this is the optimum location to attach sensors for fall detecting as mentioned in previous studies. Threshold-based analysis for acceleration magnitude, vertical velocity estimate analysis and body posture analysis are performed with data from tri-axial accelerometer reading. Threshold based-analysis for angular velocity is performed with data from tri-axial gyroscope reading.

4.1.1 Threshold-Based Analysis for Acceleration Magnitude

Threshold-based analysis for acceleration magnitude (including impact) has been chosen as first step to detect fall event in the proposed fall detection algorithm. The threshold-based method is very useful for indication of a fall (Bourke, et al., 2007a). For reliable operation of the fall detection system, firstly the resultant signal from the tri-axial accelerometer sensor at the chest was derived by taking the root-sum-of-squares of the three signals from tri-axial accelerometer recording. Setting thresholds for each of the three axes of measurement does not work well, because it does not cover all the possible directions of impact in a uniform way. The threshold for RSS (Root-Sum-of-Squares) of tri-axial accelerometer signal has been suggested to be more accurate in fall detection than single axis thresholds (Bourke, et al., 2005).

When stationary, the root-sum-of squares signal from the tri-axial accelerometer is a constant +1*g*. As expected, the RSS signal (magnitudes of acceleration) in falling are generally greater than in normal activity such as walking, running and sitting. The root-sum-of squares signal (RSS signal) contains both dynamic and static acceleration components, is calculated from sampled data as indicated in Equation (4.1).

$$RSS= \sqrt{a_x^2 + a_y^2 + a_z^2} \tag{4.1}$$

Where a_x, a_y, a_z is the acceleration (*g*) in the x, y and z axes, respectively.

Lower Fall Threshold (LFT) and Upper Fall Threshold (UFT) of acceleration have been used to detect the fall by examining recorded values of RSS signal. The lower and upper thresholds for the acceleration used to identify the fall are derived as follows:

- Lower fall threshold (LFT): means that the negative peaks for the resultant of each recorded activity are referred to as the signal lower peak values (LPVs). The LFT for the acceleration signals is set at the level of the smallest magnitude lower fall peak (LFP) recorded. The LFT is related to the acceleration of the chest at or before the initial contact of the body segment with the ground.

- Upper fall threshold (UFT): means that the positive peaks for the recorded signals for each recorded activity are referred to as the signal upper peak values (UPVs). The UFT for each of the acceleration signals is set at the level of the smallest magnitude UPV recorded. The UFT is related to the peak impact force experienced by the body segment during the impact phase of the fall.

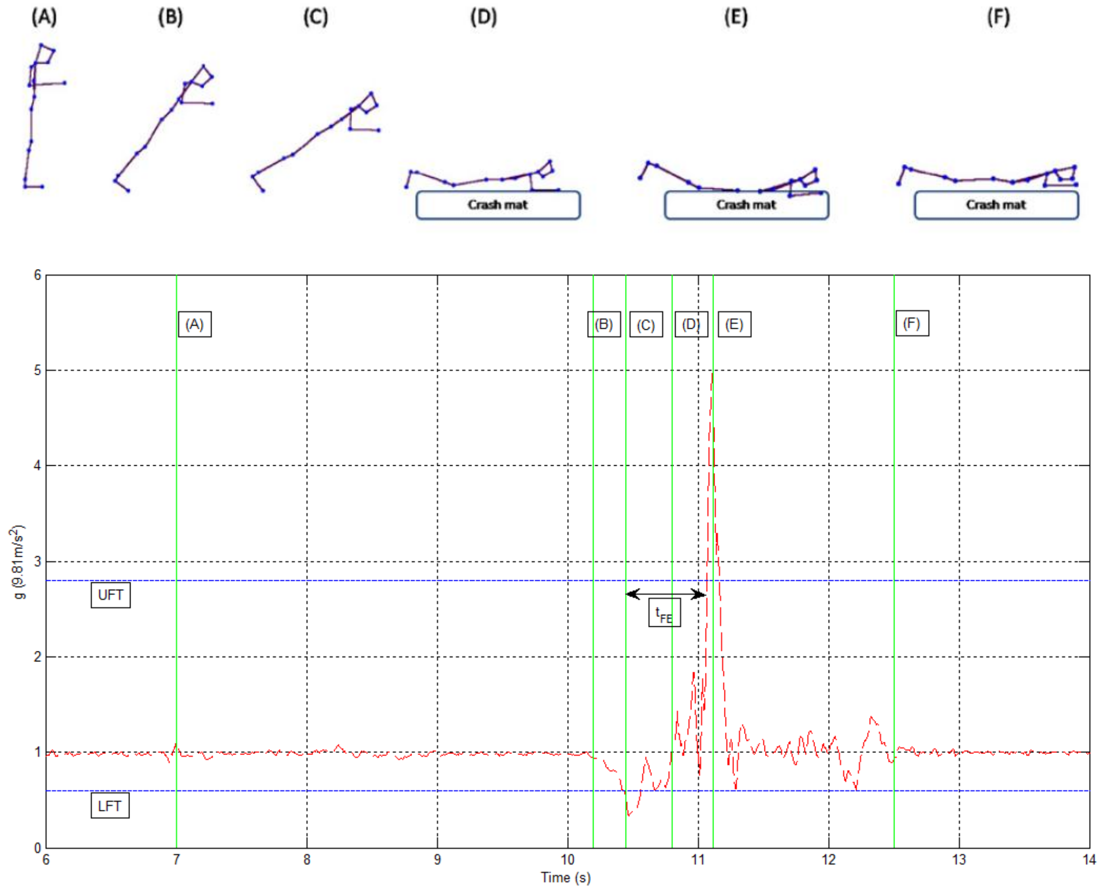

Figure 4.2 Anatomy of a fall

Figure 4.2 shows that an example of the general contour of the Root-Sum-of-Squares (RSS) signal recorded from the tri-axial accelerometer signals, during a fall from standing height. When stationary the RSS signal measures +1g, point(A), as the person falls entering the ''critical phase or pre-impact phase'', (B) and (C), the RSS signal produces a lower peak as the body is in a temporary period of ''flight'' during which the downward vertical velocity increases. When the body initially contacts the ground the dynamic acceleration will be zero as the body is no longer accelerating and has reached maximum negative vertical velocity, the RSS signal returns to +1g (D). The person now sinks into the mat and experiences a deceleration, maximum deceleration occurs at (E) as the body sinks further into the mat and maximum deformation of the body and mats occurs. After this the body now enters the ''post-fall'' phase, where the body eventually settles to rest (F). The falling-edge time, t_{FE}, is from the RSS signal last going below the lower fall threshold (LFT) until it exceeds the UFT.

Fall-associated impacts have been detected with the threshold-based method for high acceleration (Karantonis, et al., 2006; Bourke, et al., 2010b) or a rapid change in acceleration (Yoshida, et al., 2005). The threshold is set based on empirical data. The smallest acceleration measured from a fall was about 3*g*, but usually ranged up to 7-10*g*'s and higher. Normal activity usually does not exceed 3*g*, but occasionally may during some rigorous movements, for example in jumping, running or sitting down suddenly. Since there is some overlap in the ranges of the acceleration magnitude between activities daily living and falling. Although past research has achieved some significant results, the accuracy is still below desired levels. So, addition approaches are needed to distinguish falling from normal activity for a more robust algorithm. From this point of view, vertical velocity estimate, body posture and threshold based-analysis for angular velocity have also been used to detect fall event more correctly and to increase accuracy of the proposed fall detection algorithm. Vertical velocity estimate, body posture and threshold based-analysis for angular velocity are given detailed for detecting fall in this chapter.

4.1.2 Vertical Velocity Estimate Analysis

Vertical velocity (pre-impact velocity) before the impact has been used to distinguish falls from ADL. Monitoring the vertical velocity instead of acceleration is used to determine activities where high acceleration values but low velocities are generated, for example, when lying down, sitting down, or walking the stairs. Threshold of vertical velocity is also a positive indication of a fall event.

(Wu, et al., 2000) showed, with a video analysis of markers placed on the subject, that vertical and horizontal speeds are three times higher during a fall than for any other controlled movement. She also showed that both speeds will increase near simultaneously during a fall whereas they are strongly dissimilar during "controlled" movements. However it has been argued by (Degen, et al., 2003) and proven by (Bourke, et al., 2008) that threshold of the vertical velocity of the trunk alone is sufficient for fall detection.

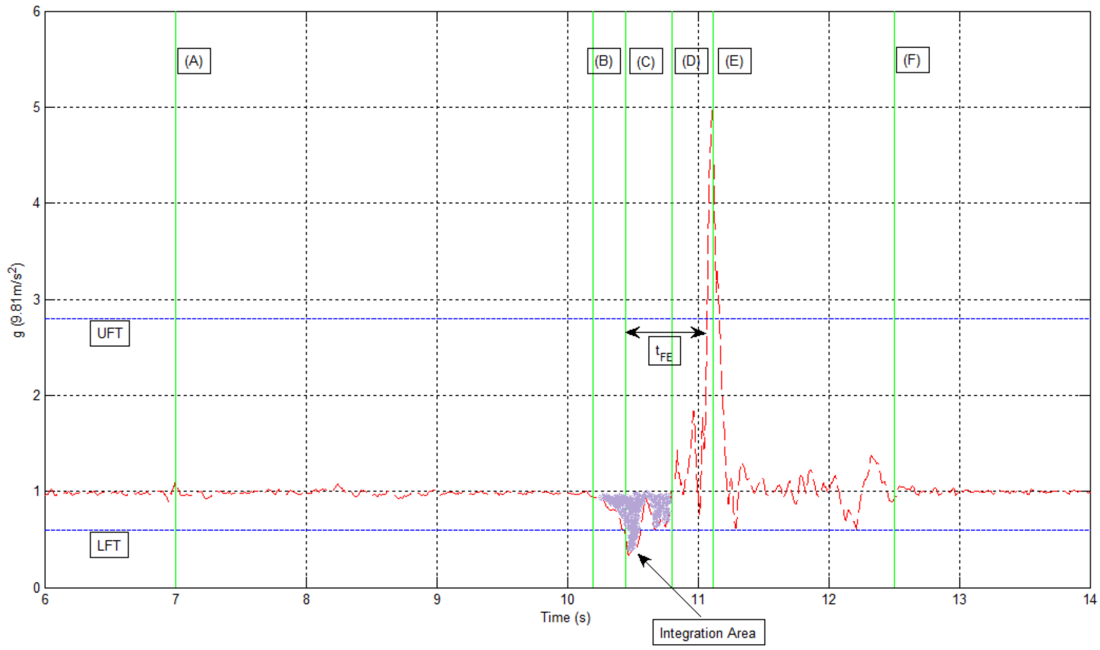

Figure 4.3 Integration areas to calculate vertical velocity

The proposed wearable fall detection monitoring system uses a tri-axial accelerometer to provide vertical velocity measurements. By integrating the area in dark shown in Figure 4.3 the pre-impact velocity from the free fall can be measured. The fall-associated impact is detected as a high peak in signal. It has previously been suggested by (Degen, et al., 2003) that vertical velocity can be approximated from a tri-axial accelerometer by numerical integration of the RSS (Root-Sum-of-Squares) of the tri-axial accelerometer signals after the magnitude of static acceleration (gravity: 9.81m/s^2) is subtracted, Equation 4.2. In this study, Degen's algorithm has been used to determine vertical velocity.

$$V_{ve} = \int \left(\sqrt{a_x^2 + a_y^2 + a_z^2} - 9.81 \right) dt \tag{4.2}$$

Where a_x, a_y, a_z is the acceleration (*g*) in the x, y and z axes, respectively and V_{ve} is vertical velocity estimate.

This approximation is only correct for vertical movements and worst for nearly horizontal movements. This approximation can be more problematic when fast accelerated movements towards the ground (acceleration ≥ 9.81m/sec^2) result in an incorrectly estimated velocity. However, this approximation has some beneficial properties. It is independent of the orientation and even rotation of wearable fall detection monitoring system.

RSS signal can only be smaller than $9.81 m/sec^2$ during a fall due to the static acceleration. Only negative values are integrated during fall. Other movements are not important except vertical movements. The implemented algorithm integrates negative values and damps the integral during positive values by using following Equation (4.3):

$$V_{ve}=\int \left(\sqrt{a_x^2 + a_y^2 + a_z^2} - 9.81 \right) dt \quad \text{if} \quad \sqrt{a_x^2 + a_y^2 + a_z^2} < 9.0$$

$$V_{ve}=V_{ve}*0.95 \qquad \text{else} \qquad (4.3)$$

A value of 9.0 is subtracted instead of the full value of $9.81 msec^{-2}$ to prohibit the integration of possible offsets and the noise of the tri-axial accelerometer. The value of 0.95 is the damping factor which removes integration drift and slowly resets the integral during rest and positive accelerations.

4.1.2.1 Numerical Integration

There are a number of discrete integration algorithms available to perform integration numerically. The acceleration signal is sampled, making it a discrete function of time having a sampling frequency, f_s, associated with it. The simplest way to perform numerical integration is to use the rectangular integration method. This method uses an accumulator to sum all past sampled inputs and the current input sample and divide by the sampling rate. Rectangular integration is represented by following difference Equation 4.4.

$$y(n)= \frac{1}{f_s}\sum_{k=0}^{n} x(n-k) = y(n-1)+ \frac{1}{f_s}\, x(n) \qquad (4.4)$$

Where x is the integrand, y is the output of the integrator, and f_s is the sampling frequency.

Another numerical integration method uses the trapezoidal rule. The results are more accurate with this method than with the rectangular method. The difference equation for trapezoidal integration is:

$$y(n)=y(n-1)+\frac{1}{2f_s}\left[x(n-1)+x(n)\right],\ \ n>0 \tag{4.5}$$

In Figure 4.4 below, a 1Hz sine wave is integrated using both methods, and clearly the trapezoidal method is more accurate in approximating the area under the curve.

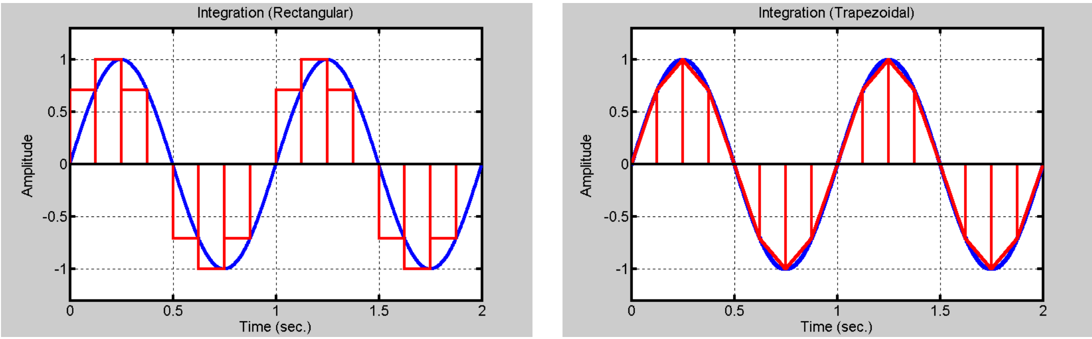

Figure 4.4 Integration using rectangular and trapezoidal methods

Trapezoidal method has been chosen for numerical integration to find vertical velocity from RSS (Root-Sum-of-Squares) of the tri-axial accelerometer signals.

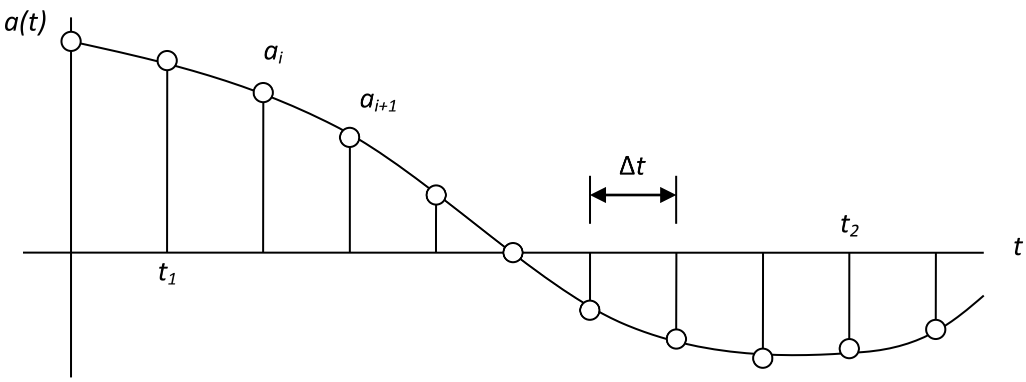

Figure 4.5 Discrete acceleration values

A simple way to approximate the area under the curve between any two points is as a trapezoid, with area $(1/2)(a_i + a_{i+1})\Delta t$ shown in Figure 4.5. Adding these areas from some time t_1 to another time t_2 gives

$$v(t_2) - v(t_1) = \int_{t_1}^{t_2} a(t)dt \approx \sum_{t_1}^{t_2} \frac{1}{2}(a_i + a_{i+1})\Delta t \tag{4.6}$$

This numerical integration technique is called the Trapezoidal Rule.

4.1.2.2 Integration Drift

It is a well-known fact that the use of numerical integration of acceleration/angular rate information from inertial sensors (accelerometers/gyroscopes) to obtain velocity/position/orientation information inherently causes velocity/position/orientation errors to grow with time, which is commonly known as "integration drift".

Unfortunately, accelerometers have an unwanted phenomenon called drift associated with them caused by a small DC bias in the acceleration signal. Ideally, there should be no DC bias from the accelerometer for the measurement of a vibration. A vibration occurs around a fixed point and has a zero mean over time. The presence of drift can lead to large integration errors. If the acceleration signal from a real accelerometer was integrated without any filtering performed, the output could become unbounded over time.

To solve the problem of drift, a high-pass filter may be used to remove the DC component of the acceleration signal. The frequency response of the filter must have a very low cutoff frequency compared to the bandwidth of the signal. By filtering before integrating, drift errors are eliminated. In this study, averaging filter has been performed for both tri-axial accelerometer and gyroscope values to eliminate the integration drift.

4.1.3 Body Posture Analysis

Body posture can be determined as an angle between the acceleration axis and gravity, by extracting the static gravitational component from the acceleration (Karantonis, et al., 2006) or by taking the dot product of the reference gravity vector and the current gravity vector (Bourke, et al., 2010b). Fall-associated posture is determined as a change in the posture before and after the impact (Boissy, et al., 2007; Yoshida, et al., 2005) or as the end posture a few seconds after the fall associated impact (Karantonis, et al., 2006; Tamura, 2005; Yoshida, et al., 2005). The recovery from a fall is recognized as an upright posture or as a certain amount of activity after a possible fall event (Karantonis, et al., 2006). The durations of posture changes from sitting to standing or from lying to standing were 3.5 and 6.0s in a group of healthy 80- to 86-year-old people (Yoshida, et al., 2005). The recovery after a fall probably takes even a lot longer than indicated above.

Postural orientation refers to the relative tilt of the body in space. In his application has aimed to provide a distinction between the upright postures of sitting and standing, as well as the various sub postures associated with lying (Karantonis, et al., 2006). When determining postural orientation, only the gravitational component of the tri-axial accelerometer signal is used because they are dealing with static accelerations where tilt is measured.

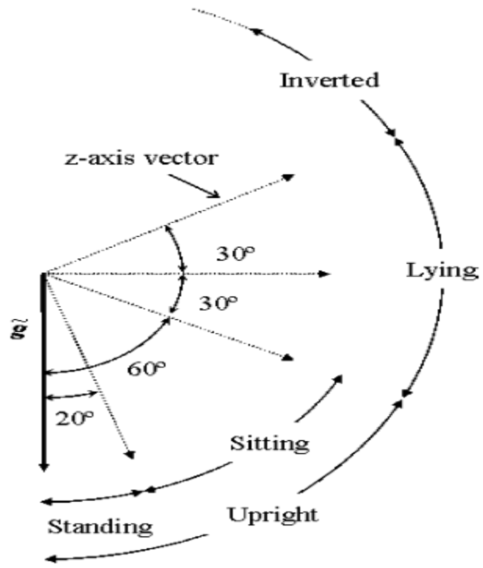

Figure 4.6 Method for determining the body posture of the faller (Karantonis, et al., 2006)

An overview of how the tilt angle relates to the various postural orientations is illustrated in Figure 4.6. If the faller's tilt angle is 0º to 60º, it is classified as upright, whereas values of 60º to 120º indicate a lying posture; any greater a tilt angle and the user is classified as inverted. If the tilt angle between 20º and 60º may be sitting and angles of 0º to 20º may be either sitting or standing, depending on various other parameters.

The technique is simple and feasible to distinguish sitting, standing and lying compared with other studies that have used neural networks, rule-based classifiers, and/or knowledge of future events. Only disadvantage of this technique is system constraints for the tri-axial accelerometer unit.

In this study, body posture (post-fall posture) has been performed by taking the dot product of the reference gravity vector, $\vec{g}_{REF}$, and the current gravity vector estimate relative to the body segment, $\vec{g}_{SEG}(t)$ as shown in Equation 4.7 and Figure 4.7.

$$\theta(t) = \cos^{-1}\left(\frac{\vec{g}_{SEG}(t).\vec{g}_{REF}}{|\vec{g}_{SEG}(t)|\,.|\vec{g}_{REF}|}\right)\ \frac{180}{\pi} \quad \text{(degrees)} \tag{4.7}$$

$\vec{g}_{REF}$ is the reference gravity vector ($\vec{g}_X$, $\vec{g}_Y$, $\vec{g}_Z$).

If the dot product angle, $\theta(t)$, between 20º and 60º may be sitting and angles of 0º to 20º may be either sitting or standing. If the inclination angle is 60º to 120º, it indicates a lying posture.

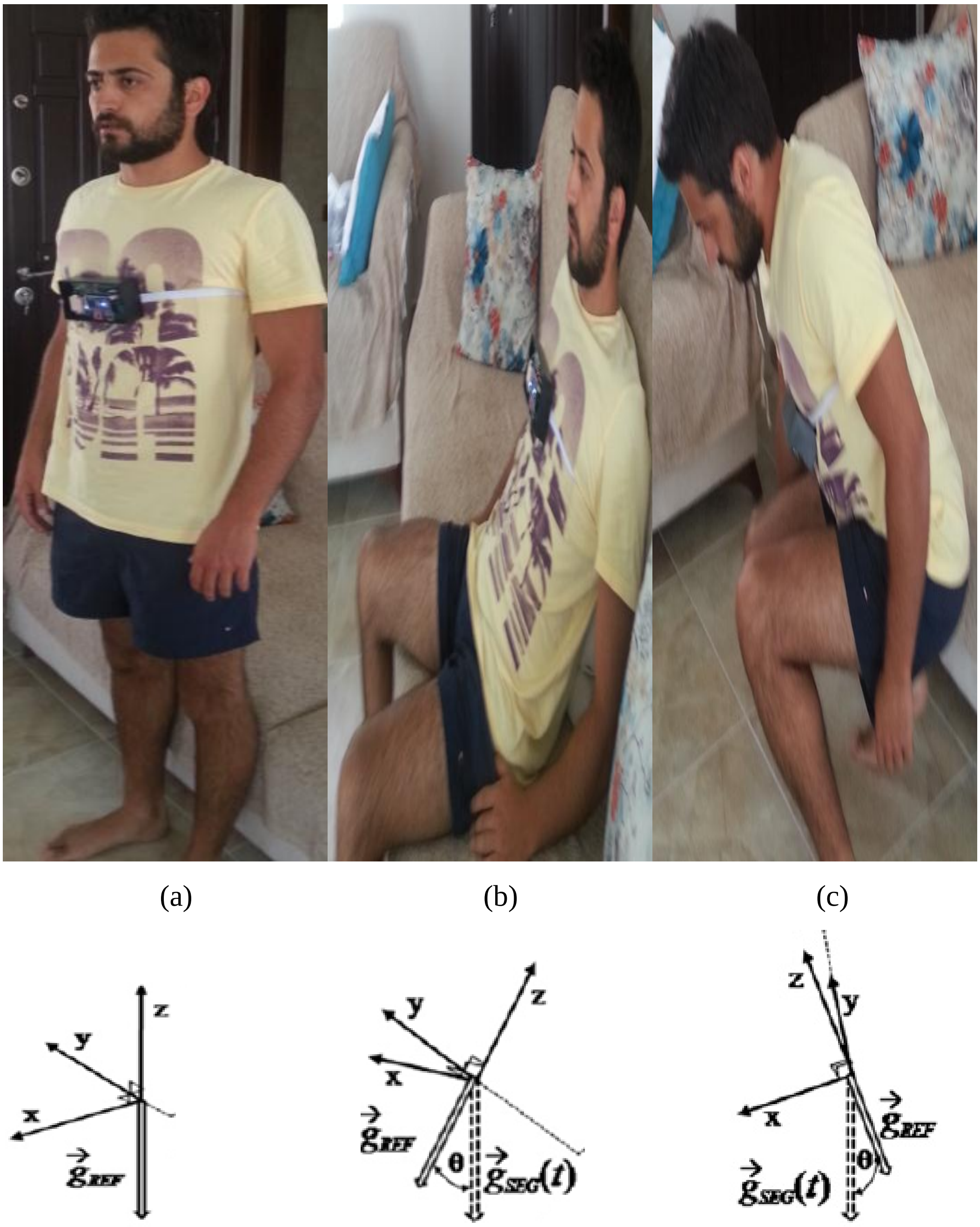

Figure 4.7 Graphical operation of the method for determining chest posture angle (a) Standing (b) Sitting and (c) Kneeling

4.1.4 Threshold-Based Analysis for Angular Velocity

Angular velocity is determined using tri-axial gyroscope sensor mounted on the chest of faller. The tri-axial gyroscope measures angular velocities x (roll), y (pitch), and z (yaw) axes.

This section describes the development of a threshold based analysis for angular velocity, capable of automatically discriminating between falls and ADL, using a tri-axial gyroscope sensor. When a person falls and hits the ground it is expected that the changes in angular velocity would be different from those experienced during normal daily activities.

The resultant vector for the angular velocity signal (ω_{res}) is derived by taking the root-sum-of-squares of angular velocities x (roll), y (pitch), and z (yaw) axes.

$$\omega_{res} = \sqrt{\omega_x^2 + \omega_y^2 + \omega_z^2} \tag{4.8}$$

Where ω_x, ω_y, ω_z is the angular velocity (degree/second) in the x, y and z axes, respectively.

When stationary, the root-sum-of squares signal from the tri-axial gyroscope which angular velocity is 0º/s. When the subject falls, the angular velocity produces a variety of signals along fall direction.

4.2 Fall Detection Algorithm

The proposed fall detection algorithm that has been developed conceptually had to be converted from a linear flowchart design to mbed programming, which runs in a while looping architecture. Because of the limited memory (64 KB SRAM) of the NXP Cortex-M3 microcontroller LPC1768, software of wearable fall detection monitoring system can record accelerometer and gyro data on the local file system. In other words, it makes it possible to record accelerometer and gyro output data to the flash specific part that is connected to the interface chip.

To ensure the program knows the ‘previous state’ of the algorithm or if one of the thresholds has been broken in a previous loop execution, a ‘trigger’ system has been used. In other words, when some thresholds have been broken a Boolean ‘trigger’ variable would be set true; in the next loop execution this would lead to additional decision statements and possible trigger activation/deactivation until all triggers are set true and a fall is detected or all triggers are turned off.

4.2.1 The Proposed Fall Detection Algorithm

The proposed fall detection algorithm shown in Figure 4.8 is based on four steps: threshold-based analysis for acceleration magnitude, vertical velocity estimate analysis, body posture analysis, and threshold based-analysis for angular velocity.

When stationary the RSS signal measures $+1g$. When a person falls entering the ''critical phase or pre-impact phase'', the person experiences a momentary free fall and reduction in acceleration magnitude. As a result, RSS signal produces a lower peak value. Firstly, the algorithm checks whether the lower peak value of RSS signal breaks LFT (Lower Fall Threshold) value or not. If this LFT is broken, first trigger will be set to true. Also, downward vertical velocity increases continuously during freefall period. Secondly, the algorithm checks whether this vertical velocity breaks vertical velocity estimate threshold (V_{ve}) within falling-edge time (t_{FE}) or not. Falling-edge time (t_{FE}) and vertical velocity estimate (V_{ve}) threshold values are determined from recorded datasets performing scripted fall and unscripted normal ADL. If this vertical velocity estimate (V_{ve}) threshold is broken within falling-edge time (t_{FE}), second trigger will be set to true. When person contacts the ground at the end of the freefall period, large spike in acceleration magnitude occurs. To detect the spike in acceleration, thirdly the algorithm checks whether the upper peak value of RSS signal breaks UFT (Upper Fall Threshold) value within falling-edge time (t_{FE}) or not. If this UFT of acceleration is broken, third trigger will be set to true. In this study, LFT and UFT of the acceleration have been used in the combination with the UFT of the angular velocity to perform the fall detection. To detect change of angular velocity, fourthly the algorithm checks whether the upper peak value of ω_{res} signal breaks UFT value within falling-edge time (t_{FE}) or not. If this UFT of angular velocity is broken, fourth trigger will be set to true. The time t=0 ms (t_0) refers to the exact time when LFT is broken by the RSS signal. Lying is detected if the body posture $\theta(t)$ exceeds 60º from t_0+1s to t_0+3s. So, if the value of $\theta(t)$ is in between

60º and 120º within t_0+1s to t_0+3s, the algorithm decides that this indicates lying posture. Thus, fifth trigger will be set to true. The algorithm then examines to see if that body posture remains after 10s, which would indicate the person is lying in their fallen position on the ground. If this holds true, the algorithm recognizes this as a fall. A failure of any of the intermediate decision conditions would reset the triggers and send the algorithm back to the start.

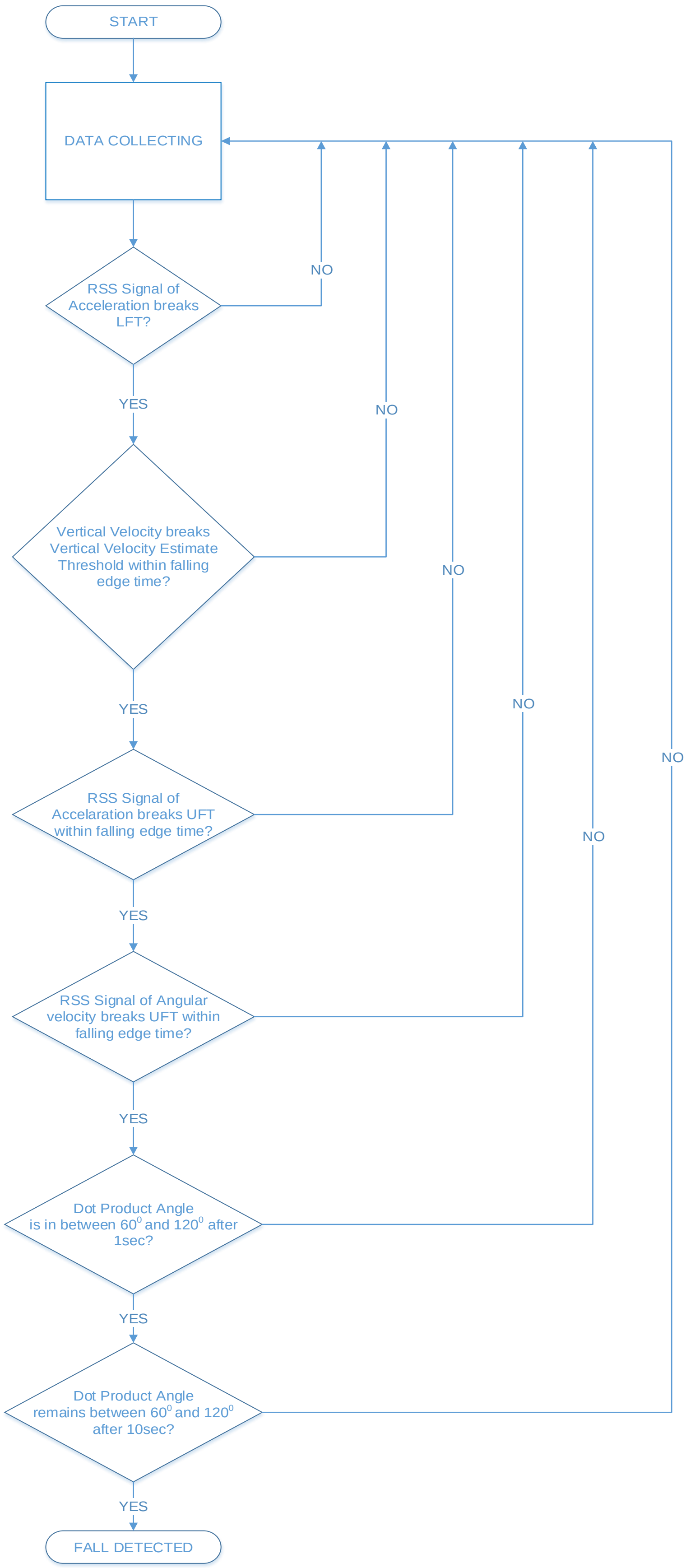

Figure 4.8 The proposed fall detection algorithm

CHAPTER FIVE
SIMULATION RESULTS

5.1 Recording and Experimental Set-up

The proposed wearable fall detection monitoring system is held in place using a standard elastic belt and commercial plastic case. The system includes a tri-axial accelerometer, tri-axial gyroscope, Bluetooth, GPS module, Vodafone vodem, microcontroller unit and buzzer & led & battery & button.

Figure 5.1 Recording and experimental set-up

Sensors readings have been recorded during intentional falls by young volunteers and ADL performed by young volunteers, middle-aged volunteers and elderly volunteer shown in Figure 5.1. The sensors readings have been recorded to flash specific part that is connected to the interface chip. The sensor signals have been sampled at 125 Hz; each signal has been averaging filtered with a length of 4 samples to avoid noise and very fast acceleration peaks, such as knock, before any further analyses. The sampling frequency of 125 Hz has been chosen because it has been shown to be high enough for sensor data analysis in fall-related motions (Karantonis, et al., 2006; Mathie, et al., 2004a).

In addition, the system uses Bluetooth module to send the real-time data to a computer. Sensors data collected during tests have been processed in a virtual environment in a computer using Matlab. The collection data program was written in Matlab. The program receives and displays real-time data from the wearable fall detection monitoring system. Also, the program continuously plots the fall detection algorithm parameters such as magnitude of acceleration, vertical velocity, angular velocity and dot-product angle for body posture from saved data in flash memory.

5.2 Intentional Falls and Sequential ADL in a Laboratory Environment

This study has determined fall detection algorithm for detection of fall phases in order to discriminate between falls and ADL. The sensitivity, specificity and accuracy of the fall detection algorithm using intentional falls and ADL in a laboratory environment were evaluated. This study has evaluated the fall detection algorithm for a chest-mounted accelerometer-gyroscope based system. The fall detection algorithm has been tested against a comprehensive data-set recorded from 5 young healthy volunteers performing 120 intentional falls and 120 scripted activities of daily living (ADL), 2 middle-aged healthy volunteers performing 48 scripted activities of daily living (ADL) and 1 elderly healthy volunteer performing 24 scripted ADL and 2.0 waking hours of continuous unscripted normal ADL. The proposed wearable fall detection monitoring system is located to the volunteer’s chest area to perform all tests.

8 intentional falls and 8 ADL have been performed for 5 healthy male volunteers, each repeated 3 times (120 falls and 120 ADL). Volunteers ranged from 25 to 28 years, body mass 66 to 85kg and height from 1.74 to 1.94m. Intentional falls in all directions (forward, backward, right-side and left side) with both legs straight and with knee flexion have been performed in a laboratory environment. The ADL have

been performed walking (10m), running (50m), lying down and standing up from a bed, sitting down and standing up from a toilet seat, sitting down and standing up from an armchair, getting in and out of a car seat, bending to pick up an object from ground, climb up stairs and go down the stairs.

2 middle-aged healthy volunteers, 1 woman and 1 man, were recruited for the study, the volunteers ranged in age from 54 to 57 years, body mass from 75kg to 82kg and height from 1.68m to 1.74m. Tests on middle-aged healthy volunteers using scripted activities have been performed at the volunteers' own homes.

An elderly (>65 years) healthy volunteer, 1 woman, was recruited for the study, the volunteer's age is 76 years, body mass is 65kg and height is 1.60m. Tests on elderly healthy volunteer using continuous scripted and unscripted activities have been performed at the volunteer's own homes.

The eight scripted ADL recorded for middle-aged and elderly healthy volunteers are the same as for young healthy volunteers except running (50m): walking (10m), sitting down and standing up from an kitchen chair, lying down and standing up from a bed, sitting down and standing up from a toilet seat, sitting down and standing up from an armchair, getting in and out of a car seat, bending to pick up an object from ground, climb up stairs and go down the stairs. Each activity is performed three times (72 ADL in total).

The elderly healthy volunteer performed continuous unscripted normal ADL in own daily life. The volunteer carried out their normal activities, including sitting, climbing stairs, lying, walking and dining during recording data. A total of 2.0 hours of activity were recorded.

Fall detection studies were mainly applied for younger volunteers performing all intentional falls designed to mimic typical fall scenarios among the elderly. However, this can cause that recorded data-set is different from general unintentional falls. Because, younger people might use preventative strategies to compensate high fall associated impacts, older people typically have less control over the speed of their body movements and longer reaction time due to reduced muscle strength with old age. Preventative strategies consist of the use of arms or knees to brake the body during fall, bending the knees, ankles and hip to decrease vertical velocity and impact force. As supported by Robinovitch, et al., (2004), self-initiated (intentional) falls result in lower vertical velocities and differences in impact sites when compared to unintentional falls. Unintentional falls produce higher velocity and peak accelerations than intentional falls. This situation is advantage to discriminate unintentional falls and ADL easily for the proposed fall detection algorithm. Also, it leads to increased true positives.

For this study, sensor data from body movements have been collected in a laboratory environment and in real life. The test protocol for intentional falls has been chosen to include typical fall type categories of older people (DeGoede, et al., 2003; Lehtola, et al., 2006; Luukinen, et al., 1994). Young healthy volunteers performed forward fall, backward fall, right sideway fall and left sideway fall. All intentional falls have been performed with both legs straight and with knee flexion. Volunteers received short instructions for performing the test falls. In this study, before performing intentional falls volunteers are instructed not to try using their hands or knees to reduce the major impact at the chest and not to take recovery steps to prevent the fall. The intentional falls have been documented using a digital video camera.

5.3 Test Results

This study has determined an accelerometer-gyroscope based method for detection of fall phases in order to discriminate between falls and ADL. In general, past research has achieved some significant results using only acceleration thresholds, but disadvantage of the idea is that there is overlapping between falls and ADL. So, accuracy is still below desired levels.

Our test results showed that even if the different parameters measured from the chest, the measuring system gives typical characteristics for intentional falls and ADL thus the value ranges had some overlapping. This indicates that using a simple acceleration threshold for impact alone is not optimal solution for practical fall detection. This is contrary to the report of (Bourke, et al., 2007a) where they were able to determine a simple acceleration threshold value for impacts capable of discriminating between intentional falls and ADL with 100% sensitivity and specificity. By taking into consideration, the proposed wearable fall detection monitoring system employs vertical velocity estimate analysis and body posture analysis using accelerometer together with threshold based analysis for acceleration magnitude. Also, threshold based analysis for angular velocity has been performed using gyroscope for discriminating falls from high density ADL (running, sitting quickly, bending).

The value ranges of dot product angle ($\Theta(t)$), vertical velocity estimate (V_{ve}) measured from the chest had specific value ranges for falls and ADL with no overlapping. Thus, these analyses were able to discriminate between falls and ADL with specificity of 100%. However, body posture analysis is included in fall detection algorithms for the chest-worn application in order to certify high sensitivity and specificity of fall detection. Based on the data-set recorded from volunteers, thresholds of UFT and LFT of acceleration magnitude, vertical velocity estimate, UFT of angular velocity, dot product angle and falling edge time for chest-worn application have been chosen empirically for effective fall detection sensitivity and specificity. On average, the main fall associated impact was detected 0.5s after the beginning of the fall, but the time range was up to 0.8s. Thus; by observing vertical velocity estimate, the pre-impact detection of falls has been determined with an average lead time 300ms before the chest impact. This average lead time leads to launch the inflation of a wearable airbag to protect the hip and head from high fall-associated impacts (Tamura, et al., 2009).

However, our test results showed that using only UFT and LFT of acceleration magnitude might misidentify the act of some ADL as fall. These are such as high density ADL (running, sitting quickly, bending). Similarly, they showed that using only UFT of the angular velocity might misidentify the act of lying back as fall. To eliminate the possibility of misidentify high density ADL, this study combine the accelerometer with the gyroscope to improve the accuracy of the system.

Also, the maximum and minimum downward vertical velocity, $V_{ve,max}$ and $V_{ve,min}$ were recorded for each fall and ADL. The maximum downward vertical velocity recorded from all the ADL can be chosen as the threshold when discriminating falls from normal ADL. The largest $V_{ve,max}$ recorded from all the ADL performed is -0.98 m/s. A threshold of -1.0m/s has been chosen ensuring the acts of some ADL were not misidentified as fall. Also, this leads to decreased false positives and increased specificity. This threshold is compared to the smallest recorded from all the falls performed is -1.02m/s. There is a gap of 0.04m/s between largest V_{ve} for an ADL and smallest V_{ve} for a fall. Thus, this show that 100% specificity has been achieved using only vertical velocity estimate analysis when performing a total of 120 falls.

Based on our studies, the proposed fall detection algorithm detects 116 times intentional falls correctly in a total of 120 falls and failed 4 times. When failed samples were examined, changing some thresholds of analyses makes it possible to detect other 4 falls correctly. Fall detection at the chest would be reliable with the algorithm detecting UFT and LFT of acceleration magnitude, vertical velocity, UFT of angular velocity and end posture with dot product angle analysis (body posture analysis) resulting in fall detection sensitivity of 96.67% and specificity of 100% in a laboratory environment with intentional falls. The results have been supported by (Bourke, et al., 2010b), who tested sensitivity and specificity of various fall detection algorithms with intentional falls from young volunteers and samples from scripted and real life ADL among elderly volunteers.

Acceptability and usability of automatic fall detection systems in real life is still inconvenient because of their relatively big size and uncomfortable to wear. In addition, another reason of this situation is that specificity of system and false alarm rate affect the usability and acceptability of the systems among the end users. Results of Bourke et al., (2010b) show that the false alarm rate in real life is 1.37 alarms per hour with data collected during 52 usage hours by older people. Recently Bianchi, et al., (2010) tested fall detection algorithms and reported that combining the detection of pressure change with acceleration impact and posture change detection decreased the false alarm rate from 11 alarms to zero in a real-life 125-minute ADL test.

Our test results show that no false fall alarms during 2 hours of monitored continuous unscripted real-life ADL for elderly volunteer. To decrease false alarm rate, end posture with dot product angle analysis has been added to the proposed fall detection algorithm. Also, when combining vertical velocity estimate analysis and end posture with dot product angle analysis the false alarm rate decreased to zero. This would result in a false alarm rate of zero alarm per hour. Our results with real-life data from 2 hours showed an average false alarm rate of zero, which is in good advancement with the previous pilot studies.

Results show that using an algorithm that employs thresholds in acceleration magnitude, vertical velocity, body posture and angular velocity achieves 100% specificity, %96.67 sensitivity and %97.1 accuracy with a false-positive rate of zero during 2 hours. When performed tests on elderly healthy volunteer using continuous unscripted activities, results show that the algorithm is the most suitable method for fall detection.

Sample signals of walking, sit-stand, lie-stand and backward fall for young volunteer-1 (Alican) are displayed in Figure 5.2 The signals displayed are the Root-Sum-of Squares (RSS) of Acceleration Magnitude, vertical velocity estimate, dot-product angle and angular velocity.

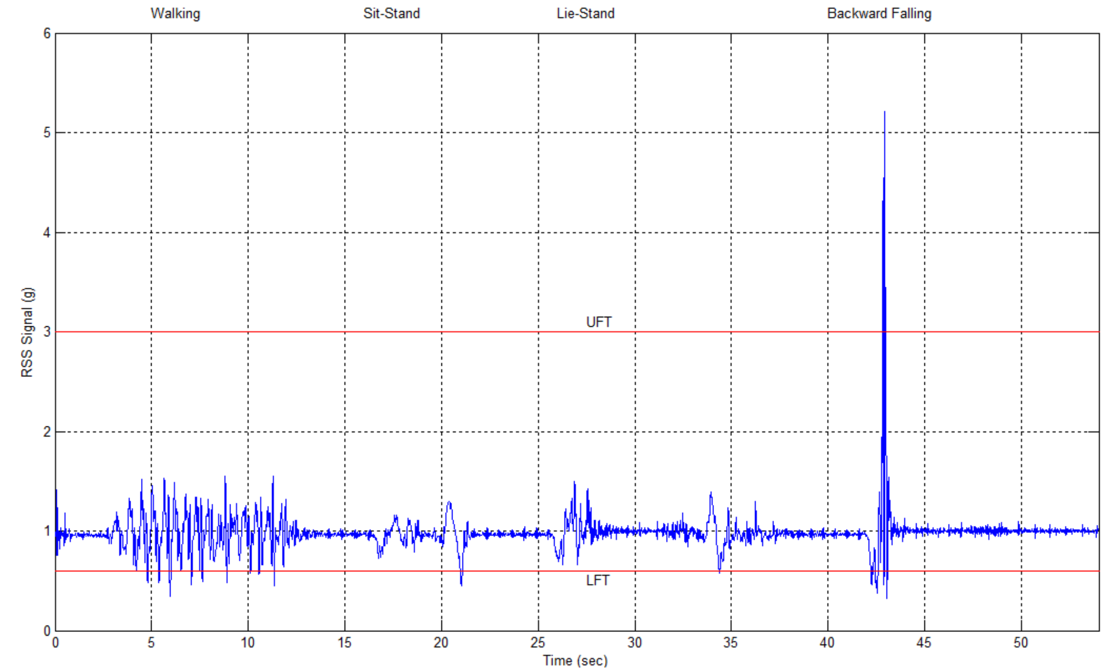
Walking
Sit-Stand
Lie-Stand
Backward Falling
RSS Signal (g)
UFT
LFT
0
1
2
3
4
5
6
0
5
10
15
20
25
30
35
40
45
50
Time (sec)

(a)

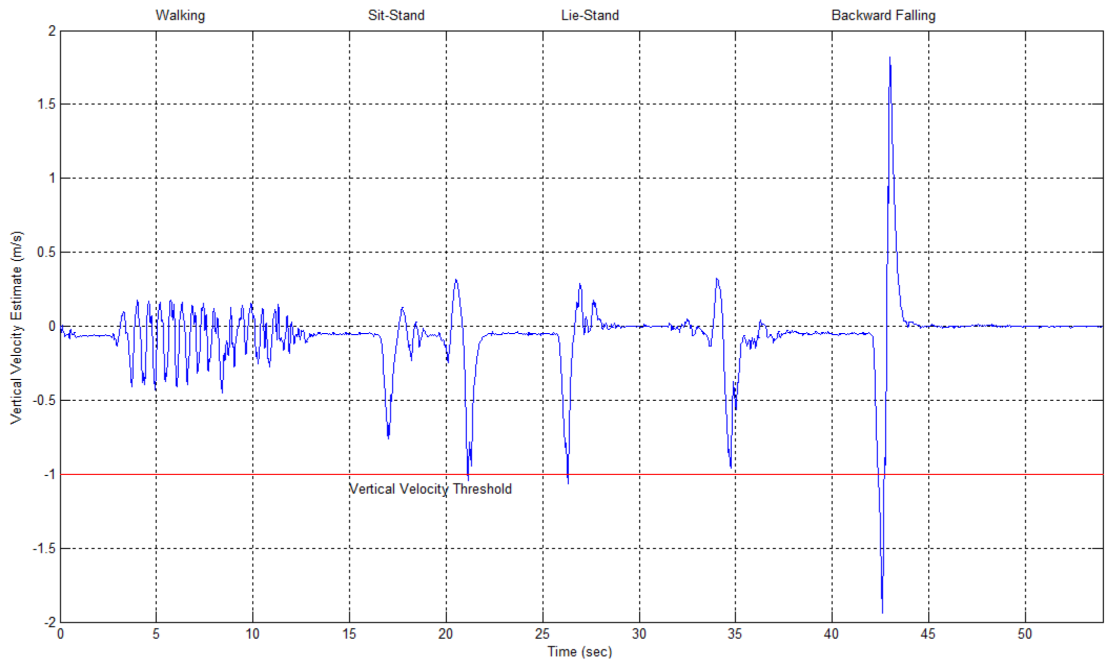
Walking
Sit-Stand
Lie-Stand
Backward Falling
Vertical Velocity Estimate (m/s)
Vertical Velocity Threshold
-2
-1.5
-1
-0.5
0
0.5
1
1.5
2
0
5
10
15
20
25
30
35
40
45
50
Time (sec)

(b)

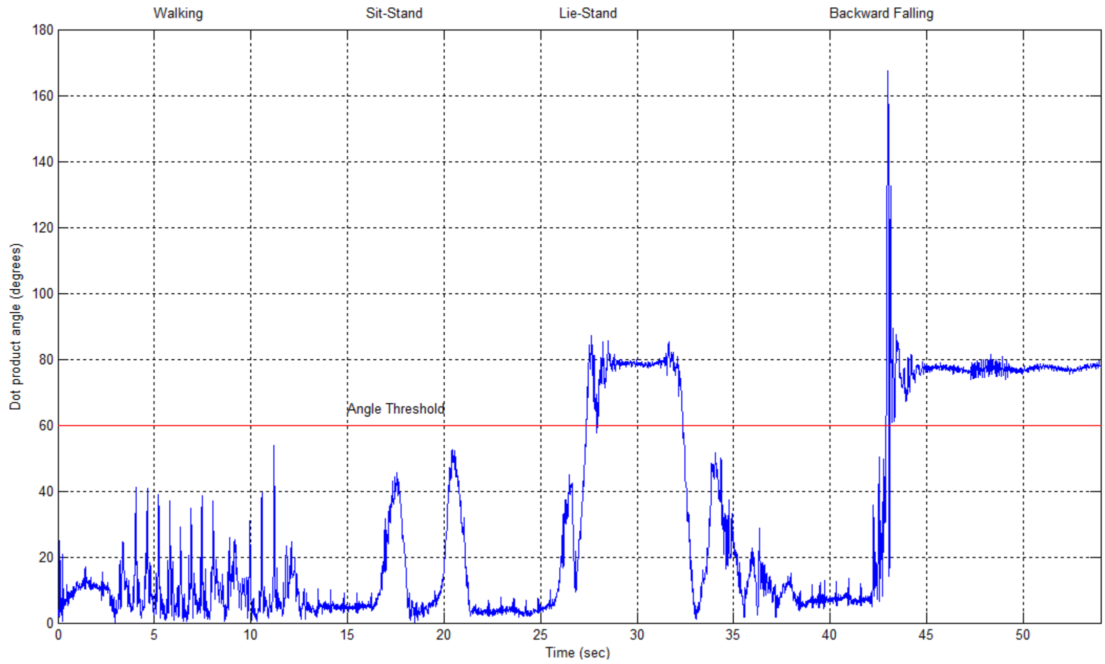

(c)

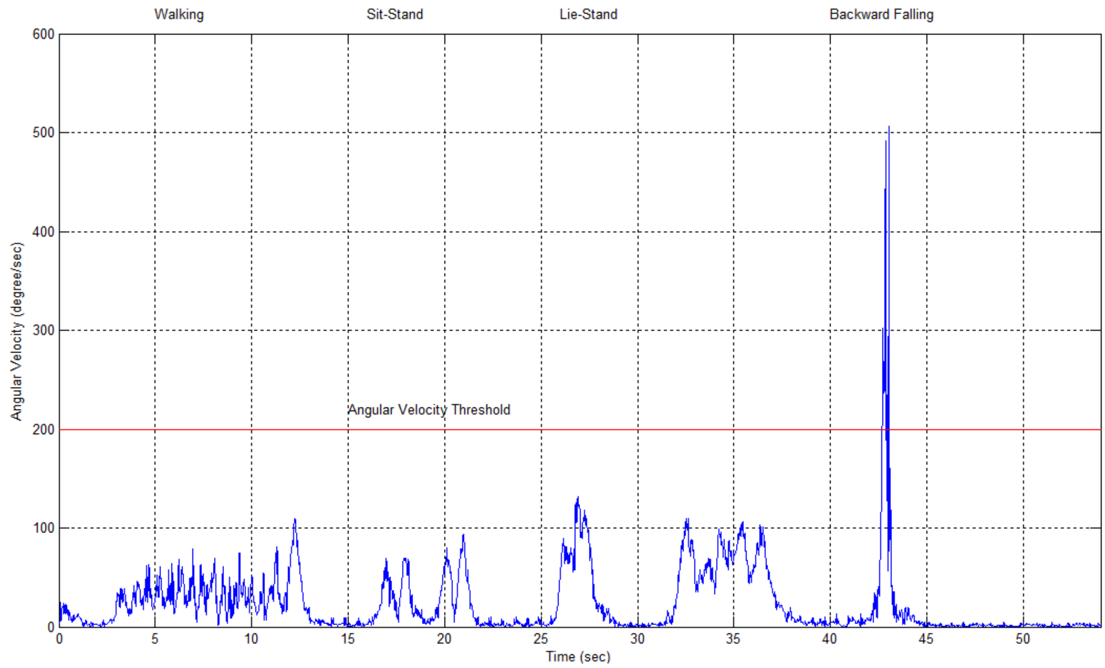

(d)

Figure 5.2 Sample signals of walking, sit-stand, lie-stand and backward fall for young volunteer-1 (Alican). The signals displayed are (a) the Root-Sum-of Squares (RSS) of acceleration magnitude, (b) vertical velocity estimate, (c) dot-product angle and (d) angular velocity.

Parameters and thresholds capable of discriminating falls and ADL have been chosen from data-set recorded from all tests. Parameters and threshold values are summarized in Table 5.1. The threshold values are adjusted to optimal detection of falls with minimized false alarms from ADL samples, i.e., maximal sensitivity with 100% specificity when possible. The thresholds are used in the proposed fall detection algorithm composed of detection of different fall phases and in evaluation of unintentional falls.

Table 5.1 Threshold values and units of the different parameters for the proposed fall detection algorithm

Threshold	Value	Unit
LFT for Acceleration Magnitude	0.6	g (9.81m/s^2)
UFT for Acceleration Magnitude	3.0	g (9.81m/s^2)
Vertical velocity estimate (V_{ve})	-1.0	meter/second (m/s)
Dot product angle ($\Theta(t)$)	60	degree (º)
Falling-edge time (t_{FE})	800	millisecond (ms)
UFT for Angular Velocity	200	degree/second (º/s)

Evaluation of fall detection system is based on determining the number of falls detected (true positives TP) or not detected (false negatives FN) by the system, and the number of activity of daily living (ADL) detected (false positive FP) or not detected (true negative TN) as fall events. Based on those values sensitivity, specificity and accuracy of fall detection can be calculated as shown below. Sensitivity (Equation 5.1) represents the percentage of true falls that were correctly detected, 100% indicating that all falls were detected.

$$\text{SENSITIVITY}=\frac{\text{TP}}{\text{TP+FN}} \text{ x } 100\% \tag{5.1}$$

Specificity (Equation 5.2) is related to the percentage of false fall alarms among ADL samples, 100% indicating that no false alarms were detected. Specificity is tested with ADL, mostly collected from instructed tasks, like walking, sitting down on a chair and standing up, and lying down on the bed and getting up.

$$\text{SPECIFICITY} = \frac{\text{TN}}{\text{TN+FP}} \text{ x } 100\% \qquad (5.2)$$

Accuracy (Equation 5.3) represents the percentage of true discrimination between falls and ADL, 100% indicating 100% sensitivity and specificity.

$$\text{ACCURACY} = \frac{\text{TP+ TN}}{\text{TP + TN + FN + FP}} \text{ x } 100\% \qquad (5.3)$$

Where:

- Number of True positive (No. TP): a fall occurs, the device detects it.
- Number of False positive (No. FP): the device announces a fall, but it did not occur.
- Number of True negative (No. TN): a normal (no fall) movement is performed, the device does not declare a fall.
- Number of False negative (No. FN): a fall occurs but the device does not detect it.

Results of sensitivity and specificity values of the proposed fall detection algorithm are shown in Table 5.2. Also, false positive (FP) quantities and false positive rate (FP/hour) and false positives per day (FP/day) for the proposed fall detection algorithm tested against the recorded continuous unscripted ADL for elderly volunteer are shown in Table 5.3.

Table 5.2 Sensitivity (%) and specificity (%) values of the proposed fall detection algorithm

The Proposed Fall Detection Algorithm	
Sensitivity (%)	96.67
Specificity (%)	
Young walking 10m	100
Young running 50m	100
Young lying down and standing up from a bed	100
Young sitting down and standing up from a toilet seat	100
Young sitting down and standing up from an armchair	100
Young getting in and out of a car seat	100
Young bending to pick up an object from ground	100
Young climb up stairs and go down a stairs	100
Elderly and Middle-aged walking 10m	100
Elderly and Middle-aged sitting down and standing up from an kitchen chair	100
Elderly and Middle-aged lying down and standing up from a bed	100
Elderly and Middle-aged sitting down and standing up from a toilet seat	100
Elderly and Middle-aged sitting down and standing up from an armchair	100
Elderly and Middle-aged getting in and out of a car seat	100
Elderly and Middle-aged bending to pick up an object from ground	100
Elderly and Middle-aged climb up stairs and go down a stairs	100
Total specificity (%)	100

Table 5.3 False positive (FP) quantities and false positive rate (FP/hour) and false positives per day (FP/day) for the proposed fall detection algorithm tested against the recorded continuous unscripted ADL.

Subjects	Time (h)	The Proposed Fall Detection Algorithm
1	2.0	0
False-positive rate (FPs/hour)	0	0
False-positive rate (FPs/day)	0	0

CHAPTER SIX
CONCLUSIONS AND FUTURE WORK

The present study has confirmed that the proposed chest-worn accelerometer-gyroscope fall detection monitoring system with the proposed fall detection algorithm can be used for fall detection. The study suggests that the use of a chest-worn fall detector with the proposed fall detection algorithm provides a reliable system for discriminating falls from ADL. There are many past researches for fall detection systems, but some of them use only acceleration threshold. So, accuracy is still below desired levels. However, to increase the accuracy, the proposed fall detection solution performs different analyses related to the fall event simultaneously. The proposed wearable fall detection monitoring system is implemented to perform threshold based analysis for acceleration magnitude and angular velocity, vertical velocity estimate analysis and body posture analysis at center chest on the body for eight different types of fall. The recorded sensor data is used to evaluate the performance of the proposed fall detection algorithm. The proposed fall detection algorithm does not need complex computation, so the detection process has been implemented on microcontroller. Moreover, the proposed wearable fall detection monitoring system is automatic and real time fall detector. The algorithm makes it possible to respond quickly.

The present study evaluates intentional falls performed by young volunteers onto crash-mats, as opposed to real life hard surfaces. Recorded impact values of real life falls are higher than intentional conditions. This situation is advantage for us because it provides a greater margin for successful detection of falls in real life. Thus, the use of lowest threshold values recorded onto crash-mats will be sufficient as detection strategy. Performing falls onto hard surfaces would increase specificity by reducing the amount of false positive like misdetection of ADL as falls.

In this study, intentional falls performed from young volunteers have been used to assess the sensitivity, specificity and accuracy of the proposed fall detection algorithm. But, to gain more significant sensitivity, specificity and accuracy, further research is required to assess the performance of the proposed fall detection algorithm by performing long-term monitoring. In addition, recorded data from real life falls among elderly volunteers is required to provide advancement in this area. This is very dangerous situation for elderly volunteers so elderly healthy volunteers performed scripted and continuous unscripted normal ADL in this study. To provide advancement in this area, elderly volunteers can be monitored long-term to perform inadvertently fall in a supervised and controlled environment. In addition, increasing number of tests on intentional falls and ADL is helpful to provide more accurate results.

For future developments, all electronic components of the proposed wearable fall detection monitoring system can be mounted onto a flexible PCB and custom housing of the system can be made from soft and elastic material to minimize injury to the user should fall on it. Material of custom housing should be robust enough to absorb impact and endure the user's weight when user falls on it. Also, flexible PCB has all electronic components together with custom housing can be woven into a tightly fitting garment on any part of body such as thigh, shoulder and head. By this way, all system should be small enough and light enough to wear comfortably and not inhibit normal daily activities. Also, this system may be waterproof in case of elderly people are in bathroom because bathroom is very dangerous place has slippery ground. It is convenient place to occur fall event for elderly people.

Moreover, the proposed fall detection algorithm has difficulties in discriminating jumping into bed and fall. Optimist approach for us is that this activity is unexpected activity to perform by elderly people. Another difficult activity is falling against wall with a seated posture to detect as fall. To detect this activity as fall, other techniques may be used such as attaching sensor modules more than one place on the body.

REFERENCES

Ambient Assisted Living Joint Programme (2008). Retrieved August 8, 2014, from http://www.aal-europe.eu.

Bianchi, F., Redmond, S.J., Narayanan, M.R., Cerutti, S., & Lovell, N.H. (2010). Barometric pressure and triaxial accelerometry-based falls event detection. *IEEE Trans Neural Systems and Rehabilitation Engineering, 18*(6), 619–627.

Boissy, P., Choquette, S., Hamel, M., & Noury, N. (2007). User-based motion sensing and fuzzy logic for automated fall detection in older adults. *Telemedicine Journal and E-Health, 13*(6), 683–693.

Bourke, A.K., O'Brien, J.V., & Lyons, G.M. (2007a). Evaluation of a threshold-based tri-axial accelerometer fall detection algorithm. *Gait Posture, 26*(2), 194-199.

Bourke, A.K., Culhane, K.M., O'brien, J.V., & Lyons, G.M. (2005). The development of an accelerometer and gyroscope based sensor to distinguish between activities of daily living and fall-events. *Conference Proceedings International Federation for Medical and Biological Engineering European Conference Biomedical Engineering, 11*.

Bourke, A.K., van de Ven, P., Gamble, M., O'Connor, R., Murphy, K., Bogan, E., et al. (2010b). Evaluation of waist-mounted triaxial accelerometer based fall-detection algorithms during scripted and continuous unscripted activities. *Journal of Biomechanics, 43*(15), 3051–3057.

Bourke A.K., O'Donovan, K.J., & Olaighin, G., (2008). The identification of vertical velocity profiles using an inertial sensor to investigate pre-impact detection of falls, *Medical Engineering & Physics.*

Brownsell, S., & Hawley, M.S. (2004). Automatic fall detectors and the fear of falling. *Journal of Telemedicine and Telecare, 10*(5), 262–266.

Bueno-Cavanillas, A., Padilla-Ruiz, F., Jimenez-Moleon, J.J., Peinado-Alonso, C.A., & Galvez-Vargas, R. (2000). Risk factors in falls among the elderly according to extrinsic and intrinsic precipitating causes. *European Journal Epidemiology, 16*(9), 849–859.

Communication from the Commission to the European Parliament, the Council, the European Economic and Social Committee and the Committee of the Regions, (2007). Ageing well in the Information Society - an i2010 Initiative - *Action Plan on Information and Communication Technologies and Ageing.*

COOP-005935-HEBE, (2006). Cooperative research project – CRAFT. *Automatic fall detection and activity monitoring for elderly*. Retrieved August 8, 2014, from http://www.fatronik.com/documentos/ otraspub/Medetel_pres.pdf.

CUI Inc, (2006). *CEM-1203(42) Magnetic Buzzer*. Retrieved August 8, 2014, from https://www.sparkfun.com/datasheets/Components/CEM-1203.pdf.

Degen, T., Jaeckel, H., Rufer, M., & Wyss, S., (2003). Speedy: A fall detector in a wrist watch. *Proceedings Seventh IEEE International Symposium on Wearable Computing*.

DeGoede, K.M., Ashton-Miller, J.A., & Schultz, A.B. (2003). Fall-related upper body injuries in the older adult: a review of the biomechanical issues. *Journal of Biomechanics, 36*(7), 1043–1053.

Diaz, A., Prado, M., Roa, L.M., Reina-Tosina, J., & Sanchez, G. (2004). Preliminary evaluation of a full-time falling monitor for the elderly. *Conference Proceedings IEEE Engineering Medicine & Biology Society, 3*, 2180–2183.

Fleming, J., & Brayne, C. (2008a). Inability to get up after falling, subsequent time on floor, and summoning help: prospective cohort study in people over 90. *British Medical Journal, 337,* a2227.

GlobalSat Technology Corporation (n.d.). *EM-406 GPS Receiver Engine Board Product Guide*. Retrieved August 8, 2014, from https://www.sparkfun.com/ datasheets /GPS/EM-406%20Product_Guide1.pdf.

Gökçegöz, F. (2013). *STM8S – HC06 bluetooth modül ile haberleşme uygulamaları*. Retrieved August 8, 2014, from http://www.mcu-turkey.com/tag/hc-06-bluetooth-module/.

Gurley, R.J., Lum, N., Sande, M., Lo, B., & Katz, MH. (1996). Persons found in their homes helpless or dead. *New England Journal of Medicine, 334*(26), 1710-1716.

Heinbüchner, B., Hautzinger, M., Becker, C., & Pfeiffer, K. (2010). Satisfaction and use of personal emergency response systems. *Zeitschrift Gerontologie and Geriatrie, 43*(4), 219–223.

InvenSense Inc., (2010). *ITG-3200 Product Specification Revision 1.4,* Retrieved August 8, 2014, from https://www.sparkfun.com/datasheets/Sensors/Gyro/PS-ITG-3200-00-01.4.pdf.

Jia, N. (2009). Detecting Human Falls with a 3-Axis Digital Accelerometer. *Analog Dialogue,* 43-07.

Kangas, M. (2011). *Development of Accelerometry-based Fall Detection University of Oulu*. Retrieved August 8, 2014, from http://herkules.oulu.fi/isbn97895142967 /isbn9789514296857.pdf

Karantonis, D.M., Narayanan, M.R., Mathie, M., Lovell, N.H., & Celler, B.G. (2006). Implementation of a real-time human movement classifier using a tri-axial accelerometer for ambulatory monitoring. *IEEE Transaction on Information Technology in Biomedicine, 10*(1), 156–167.

Lehtola, S., Koistinen, P., & Luukinen, H. (2006). Falls and injurious falls late in homedwelling life. *Archives of Gerontology and Geriatrics*, *42*(2), 217–224.

Lindemann, U., Hock, A., Stuber, M., Keck, W., & Becker, C. (2005). Evaluation of a fall detector based on accelerometers: a pilot study. *Medical & Biological Engineering & Computing*, *43*(5), 548–551.

Luukinen, H., Koski, K., Hiltunen, L., & Kivelä, S.L. (1994). Incidence rate of falls in an aged population in northern Finland. *Journal of Clinical Epidemiology, 47*(8), 843–850.

Mathie, M.J., Celler, B.G., Lovell, N.H., & Coster, A.C. (2004a). Classification of basic daily movements using a triaxial accelerometer. *Medical & Biological Engineering & Computing*, *42*(5), 679–687.

Melander-Wikman, A., Jansson, M., Hallberg, J., Mortberg, C., & Gard, G. (2007). The Lighthouse Alarm and Locator trial-a pilot study. *Technology Health Care, 15*(3), 203–212.

Noury, N., Rumeau, P., Bourke, A.K., O´Laighin, G., & Lundy, J.E., (2008b). A proposal for the classification an evaluation of fall detectors. *IRBM—Ingenierie et Recherche Biomedicale/Biomedical Engineering and Research*, *29*(6), 340–349.

NXP Semiconductors (2009) *Rapid prototyping for the LPC1768 MCU*. Retrieved August 8, 2014, from http://www.nxp.com/documents/leaflet/LPC1768.pdf.

Robinovitch, S.N., Brumer, R., & Maurer, J. (2004). Effect of the squat protective response on impact velocity during backward falls. *Journal of Biomechanics, 37*(9), 1329-1337.

Sparkfun (n.d.). *Serial Communication – Rules of Serial*, Retrieved August 8, 2014, from https://learn.sparkfun.com/tutorials/serial-communication/rules-of-serial.

Suzuki, M., Ohyama, N., Yamada, K. & Kanamori, M. (2002). The relationship between fear of falling, activities of daily living and quality of life among elderly individuals. *Nursing & Health Science, 4*(4), 155–161.

Tamura, T. (2005). Wearable accelerometer in clinical use, *Conference Proceedings IEEE Engineering Medicine & Biology Society, 7*, 7165–7166.

Tamura, T., Yoshimura, T., Sekine, M., Uchida, M., & Tanaka, O. (2009). A wearable airbag to prevent fall injuries. *IEEE Transaction on Information Technology in Biomedicine, 13*(6), 910–914.

Tinetti, M.E., Speechley, M., & Ginter, S.F. (1988). Risk factors for falls among elderly persons living in the community. *New England Journal of Medicine, 319*(26), 1701–1707.

Tinetti, M.E., Liu, W.L., & Claus, E.B. (1993). Predictors and prognosis of inability to get up after falls among elderly persons. *Journal of the American Medical Association, 269*(1), 65–70.

Toulson, R., & Wilmshurst, T. (2012). *Fast and effective embedded systems design.* United Kingdom, An imprint of elseiver

Tusuzki, T., (n.d.). *Analog Devices ADXL345 Quick Start Guide*. Retrieved August 8, 2014, from http://www.analog.com/static/imported-files/application_notes/AN-1077.pdf.

Vodafone (n.d.). *K3770 Vodem*. Retrieved August 8, 2014, from http://www.vodafone.com.tr/Is-Ortagim/vodem-K3770.php.

Wu, G. (2000). Distinguishing fall activities from normal activities by velocity characteristics. *Journal of Biomechanics*, *33*, 1497–500.

Yardley, L., & Smith, H. (2002). A prospective study of the relationship between feared consequences of falling and avoidance of activity in community-living older people. *Gerontologist*, *42*(1), 17–23.

Yoshida, T., Mizuno, F., Hayasaka, T., Tsubota, K., Wada, S., & Yamaguchi, T. (2005). A wearable computer system for a detection and prevention of elderly users from falling. *Conference Proceedings Biomedical Engineering*, *12*, 179–182.